QUANTUM COHERENCE PHENOMENA IN X-RAY OPTICS

A Dissertation

by

PETR MIKHAILOVICH ANISIMOV

Submitted to the Office of Graduate Studies of
Texas A&M University
in partial fulfillment of the requirements for the degree of

DOCTOR OF PHILOSOPHY

December 2008

Major Subject: Physics

QUANTUM COHERENCE PHENOMENA IN X-RAY OPTICS

A Dissertation

by

PETR MIKHAILOVICH ANISIMOV

Submitted to the Office of Graduate Studies of
Texas A&M University
in partial fulfillment of the requirements for the degree of

DOCTOR OF PHILOSOPHY

Approved by:

Chair of Committee,	Olga Kocharovskaya
Committee Members,	Alexey Belyanin
	Yuri Rostovtsev
	Phillip R Hemmer
Head of Department,	Edward S. Fry

December 2008

Major Subject: Physics

ABSTRACT

Quantum Coherence Phenomena in X-ray Optics. (December 2008)
Petr Mikhailovich Anisimov, B.S., Nizhny Novgorod State University, Russia;
M.S., Nizhny Novgorod State University, Russia
Chair of Advisory Committee: Dr. Olga Kocharovskaya

The effects of quantum coherence in X-ray optics at nuclear transitions are investigated from a theoretical point of view. First, we introduce the general concept of the decaying dressed states and present a classification of the quantum coherence effects in a three-level coherently driven system. Second, we show that the interference effects may appear in X-ray radiation at the nuclear transitions under the condition of the nuclear level anti-crossing. This effects are similar to electromagnetically induced transparency, which has been widely studied earlier at the electronic transitions in optics. We also suggest a new technique for inhomogeneous line narrowing at nuclear transitions. This technique is based on the combined action of RF and DC fields and adopted to be applied in the Mössbauer spectroscopy. Numerical simulation of a simple model with the dipole-dipole interaction is presented in order to demonstrate the efficiency of the technique. Finally, we study the possibility to suppress the nuclear elastic forward scattering in the synchrotron experiments using trains of pulses. A numerical model is developed to confirm this possibility and the main issue of relative phases of consecutive pulses is discussed.

To my loving parents: Anisimov Mikhail Stepanovich and Spirova Lidiya Petrovna

ACKNOWLEDGMENTS

It is my pleasure to thank all those who helped me to complete this degree.

This work was performed under the supervision of Dr. Olga A Kocharovskaya, with whom it was a great privilege to work. I want to thank her for support, guidance and encouragement to work on challenging physical problems.

I am very grateful to Andrea Burzo, my girlfriend and co-worker, whose devotion to physics always served as an inspiration for me, who constantly supported and helped me both scientifically and emotionally.

I would like to thank colleagues with whom I have worked: F. Vagizov, Yu. Rostovtsev, V. Sautenkov, A. Andreev, J. Odeurs, E. Alp, S. Olariu, R. Callens. They were a great help to me in my research and from whom I benefited tremendously.

Finally, I want to thank my friends, both here and in Russia, for years of support, advice and encouragement.

TABLE OF CONTENTS

CHAPTER Page

LIST OF TABLES

LIST OF FIGURES

FIGURE Page

FIGURE Page

FIGURE Page

FIGURE Page

FIGURE Page

FIGURE Page

CHAPTER I

INTRODUCTION

Coherence is the property of a physical system which implies a maintenance of a phase relationship and manifests itself in the ability of the system to exhibit some sort of interference. Interference, in turn, is an inherent property of the waves which originates from the superposition principle. In quantum mechanics a physical system is characterized by a wave function which has a wave-like properties. The superposition principle can be applied to a wave function as well when quantum system has more than one path to evolve from the same initial to the same final state. In this case, a resulting wave function is equal to a sum of all individual wave functions corresponding to all possible evolution pathways. Hence, the ability of the wave functions of quantum system to interfere is called quantum coherence.

A specific example of quantum coherence is the atomic coherence. It is described by the off-diagonal elements of density matrix of an atom and represents itself as a coherent superposition of the different eigen states of the atomic Hamiltonian. Such coherence may be induced at the atomic transition either by resonant coherent electromagnetic radiation or by bi-chromatic radiation interacting with the adjacent atomic transitions in a multilevel system. Study of the atomic coherence/interference effects in multilevel atomic systems interacting with multi-frequency radiation has very long history. It started in 1924 with experimental observation by R. W. Wood and A. Ellet [1, 2, 3] and theoretical interpretation by W. Hanle [4] of resonance fluorescence signal depolarization by an external magnetic field in mercury vapour. That was a quantum coherence effect in the system including discrete levels. Later,

---

The journal model is *Physical Review B*.

quantum coherence effect in the system including continuum of states was studied by U. Fano [5]. Many other effects which originate from two-photon excitation of the atomic coherence were also studied. The list of the effects includes quantum [6, 7, 8, 9, 10] and Raman [11, 12] beats, Bell-Bloom resonances [13, 14], coherent population trapping (CPT) [15, 16], laser induced continuum structures [17, 18, 19], etc. For review on a subject one can read [20, 21].

In the last two decades, study of such effects as electromagnetically induced transparency (EIT) [22, 23, 24, 25], lasing without inversion [26], slow light [27], received a lot of attention forming one of the most rapidly developing fields of research in quantum optics. The simplest system in which effects can be observed is a three-level atomic or molecular system, shown in Fig. 1, interacting with two laser fields in such a way that the laser driven transitions are dipole allowed while the third transition, typically Zeeman or hyperfine, is dipole forbidden. The interference occurs between transition pathways induced by the fields within the internal quantum states of atoms and molecules. This interference leads to dramatic modifications of the optical response of the system. In particular, absorption of a probe field tuned to the resonance with some transition can be cancelled leading to an initially opaque medium being rendered transparent for the probe field. Suppression of the resonant absorption provides also the possibility for lasing without inversion [26]. A narrow transparency resonance is accompanied by the sharp dispersion leading to the possibility of manipulation of the group velocity of a light pulse propagating in the medium, i.e. to reduce it down to a few meters per second or even bring the pulse to a complete stop, imprint the quantum state carried by pulse photons into a superposition of long-lived spin states of atoms and to later retrieve it with (ideally) no losses [27], thus realizing the first steps toward optically carried quantum information storage and processing and quantum computing.

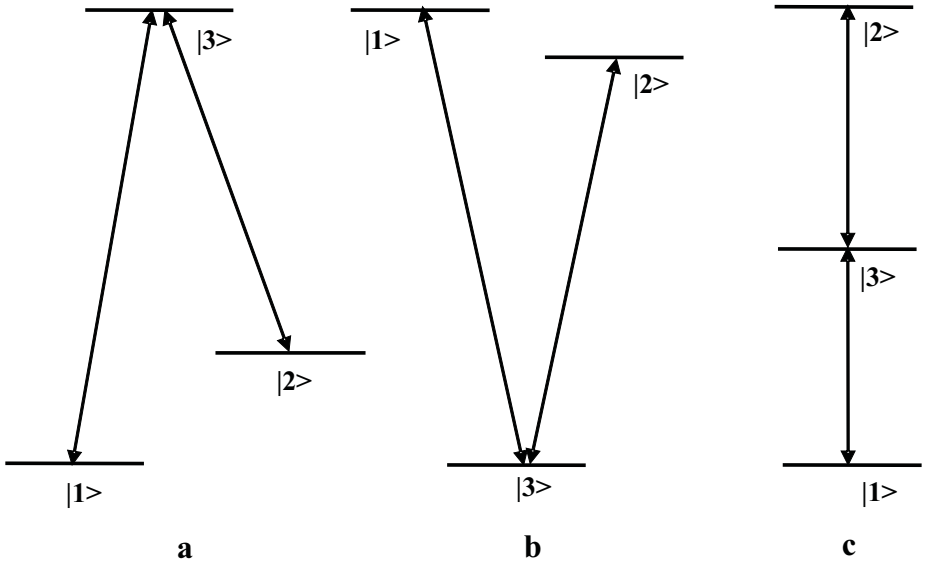

FIG. 1. Generic three-level atomic or molecular systems coupled with two electromagnetic fields in which the interference effects are most easily realized: a) Λ scheme; b) V scheme; c) ladder scheme.

The atomic coherence and resulting interference phenomena were widely studied both theoretically and experimentally in the optical range of frequencies at the electronic transitions mainly in gaseous media [20, 21, 24, 26, 27, 28] and more recently in solids [29, 30, 31, 32, 33]. Fast developing of this field is due to many promising applications such as quantum information storage and processing, efficient and low intensity wave mixing and optical switching, lasing in the traditionally "difficult" frequency ranges (such THz, VUV, X-rays), high sensitive spectroscopy, metrolodgy and magnetometry, controllable optical delay lines, etc.

The major goal of this work is to extend this field of research from optical to X-ray range of frequencies and simultaneously from the atomic to the nuclear transitions. More specifically this research is focused on studies of the quantum coherence effects at the nuclear transitions in solids in the range from about 5 keV to about 150 keV. In this range of nuclear excitations the Mössbauer spectroscopy technique provides a

convenient tool for coherent probing of the resonant nuclear absorption.

Mössbauer spectroscopy is based on Mössbauer effect (i.e. recoilless resonant absorption/emission of nuclei in sufficiently rigid crystal lattice). The transitions energies are limited from below by about 5 keV due to the internal electron conversion. For very high nuclear excitations (higher than 150 keV) the rigidity of the solid host is not sufficient to provide high enough probability of the recoilless transition.

Along with coherent probing of the resonant absorption, an observation of the quantum coherence effects at the nuclear transitions requires also sufficiently strong coherent resonant driving of the adjacent nuclear transition. Coherent radiation in different frequency ranges could be used in principle for the resonant driving of the nuclear transitions.

Unfortunately absence of the nuclear transitions in the optical range of energies does not allow for the direct nuclear excitation by lasers.[1] An interesting idea of indirect laser driving of the Mössbauer transition via resonant interaction of laser radiation with electronic transition in atom/ion and hyperfine interaction providing coupling between electron and nuclear degrees of freedom was suggested some time ago [34, 35, 36, 37]. However, the attempts of its experimental implementation in ^{57}Fe [38] and ^{151}Eu compounds [39] met a number of difficulties. First of all optical excitation of sufficiently large (for Mössbauer probing) number of ions in solids requires high power lasers which heats the sample making difficult interpretation of the data [40]. Comparison of the Mössbauer spectra taken at the same temperature in the absence and in the presence of laser radiation could be provided using pulsed excitation. However, the last one leads to the vibrations of the sample [38] which, in turn, provides

[1] Two transitions at 3.5 eV in Th-229 and 75 eV in U-239 represent an interesting exception. However both transitions are strongly forbidden with the life time of an order of several hours.

a dramatic modifications of the Mössbauer spectra making difficult separation and study of the pure electronic effects.

Hyperfine nuclear sub-levels with an energy separation of an order of 1 MHz can be efficiently driven by an RF-field [41]; see also [36, 42, 43, 44, 45] for reviews. Such effects as dynamic Stark splitting [46, 47, 48, 49], appearance of the RF sidebands in the nuclear gamma-ray absorption [50, 51, 52] and collapse of the hyperfine structure [53, 54, 55] have been predicted a long time ago and demonstrated experimentally in 90th in soft ferromagnetic films. In these materials, a strong internal magnetization follows a rather weak external magnetic field allowing for achievement of very high Rabi frequency. In the case of the nuclear level crossing strong driving of the corresponding degenerate transition could be provided by the DC-field.

Currently there are no strong coherent sources of radiation in the X-ray range of frequencies.[2] However, the synchrotron radiation is available now as a train of ultra-short pulses. It could provide under certain conditions coherent manipulation of the nuclear absorption.

All three possibilities, namely, coherent manipulation of the nuclear Mössbauer transitions by the RF-field (resonant driving of the hyperfine transitions), by DC-field (in the case of the nuclear level crossing), and by the trains of pulses from the synchrotron sources are studied in the frame of this dissertation.

The organization of the dissertation is as follows.

In Chapter II, the general concept of the decaying dressed states in three-level coherently driven system is introduced. It provides simple and straightforward classification of the coherent effects in a three-level coherently driven system. Chapter III discusses the recent experimental results of our group demonstrating suppression

[2]Hopefully at least two such sources with the wavelength of an order of 1 $\mathring{A}$ based on free electron lasers will be available in the near future at SLAC and TESLA.

of the resonant gamma-ray absorption in the thin single crystal or powder samples of ^{57}Fe in $FeCO_3$ under the condition of the nuclear level crossing. The notion of the decaying dressed states introduced in the previous chapter is used to demonstrate a crucial role of the difference in the dephasing rates of two crossing sub-levels for interpretation of the observed suppression of the resonant absorption as EIT.

In Chapter IV, a method for suppression of inhomogeneous broadening of Mössbauer absorption lines based on a combined action of the RF and DC field is suggested. The method resembles a well-known magic angle technique in the high resolution nuclear magnetic resonance spectroscopy. It does not suppress, however, hyperfine interactions but rather provides a correlation between such interaction in the ground and excited nuclear states.

In Chapter V, a possibility of suppression of the nuclear elastic forward scattering under conditions that the hyperfine splitting is multiple to the pulse repetition rate of the synchrotron radiation is analyzed.

The list of major results obtained in this dissertation is provided in the Summary.

CHAPTER II

DECAYING-DRESSED-STATE ANALYSIS OF COHERENTLY DRIVEN THREE-LEVEL Λ SYSTEM*

We introduce decaying-dressed states for a three-level Λ system driven at one atomic transition and probed at the adjacent one. These states allow for a simple interpretation and classification of various coherent effects in such a system.

A. Introduction

A three-level Λ system, driven at one transition and probed at the adjacent one, was extensively studied in the literature due to appearance of coherent effects in the system: ac-Stark splitting and electromagnetically induced transparency (EIT). See [20, 24, 28] for the reviews.

The basis of the dressed states, i.e. eigenstates of the "atom+field" Hamiltonian, is widely used for the analysis and interpretation of aforementioned effects. It is especially useful for describing an atomic system in a driving field so strong that the corresponding Rabi frequency greatly exceeds all dephasing rates in the system. In this case the dressed states define the positions of two resonances in the atomic response separated by twice the Rabi frequency. The appearance of these two resonances is well known as the Autler-Townes effect - the dynamical splitting of a bare atomic state by a strong driving field [57].

The dressed-state basis also provides a useful analogy between EIT and Fano type interference in the case of the radiative decay of the excited atomic level and

*This is a pre-print version of "Decaying-dressed-state analysis of coherently driven three-level Λ system" by Petr Anisimov and Olga Kocharovskaya from Journal of Modern Optics (In Press) [56]. Reprinted with permission by Taylor & Francis. http://www.informaworld.com

negligible decay of the two-photon coherence. Indeed, the atomic system in the dressed-state basis under aforementioned conditions is equivalent to a system with two excited atomic levels closely spaced on the scale of radiative decay. These levels decay to the same continuum and hence exhibit Fano interference [58].

However in the general case of arbitrary dephasing rates, the transformation of the original density matrix equations to the dressed-state basis does not yield much physical insight. Moreover, it complicates the analysis. At the same time, the atomic response of a strongly driven atomic system can always be (with an exception of a single bifurcation point) presented as a simple superposition of two resonances. Thus we propose to define decaying-dressed states as the states corresponding to these resonances. Such decaying-dressed states allow for transparent classification of coherent effects and visualization of the qualitative transformation of the atomic response with the variation of the parameters of the system.

B. Decaying-dressed states

In this section we define decaying-dressed states as the effective states of a system including atom, driving field and relaxation processes. The properties of the decaying-dressed states depend on the properties of the atomic system and the driving field as well as dephasing rates.

We consider a three-level Λ system driven at the $|c\rangle \rightarrow |a\rangle$ transition by a laser field $\mathrm{E_c}$ with a frequency ω_c, detuning from the atomic resonance $\Delta = \omega_{\mathrm{ac}} - \omega_{\mathrm{c}}$, and a Rabi frequency $\Omega = \mathbf{d}_{\mathrm{ac}}\mathbf{E_c}/\mathbf{2}\hbar$. The system is probed at the adjacent $|b\rangle \rightarrow |a\rangle$ transition by a weak laser field $\mathrm{E_p}$ with a corresponding Rabi frequency $\alpha = \mathbf{d}_{\mathrm{ab}}\mathbf{E_p}/\mathbf{2}\hbar$ (see Fig. 2 left).

In order to introduce the decaying-dressed states, one should start with a density

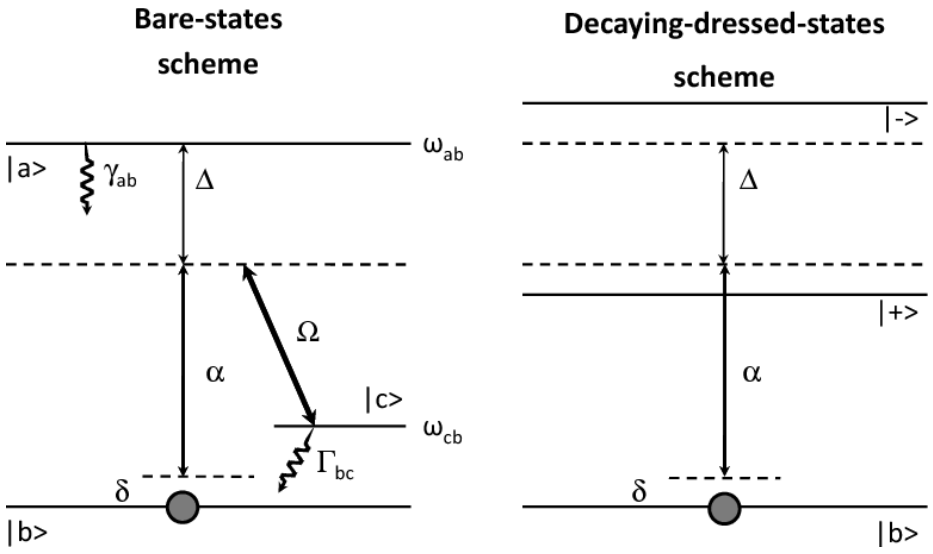

FIG. 2. Three-level Λ system coherently driven at the $|c\rangle \rightarrow |a\rangle$ transition and probed at the $|b\rangle \rightarrow |a\rangle$ transition: (left) in the bare-state basis; (right) in the decaying-dressed-state basis.

matrix formalism in a bare-state basis. We are interested in the atomic response to the weak laser field $\mathrm{E_p}$ with frequency ω_p scanned across one-photon $\omega_\mathrm{p} = \omega_\mathrm{ab}$ and two-photon $\omega_\mathrm{p} = \omega_\mathrm{cb} + \omega_\mathrm{c}$ resonances. In general, the atomic response is proportional to a slow-varying amplitude σ_ab of an atomic coherence ρ_{ab}. In the lowest order of α, all the population remains in the ground state $|b\rangle$ and the slow-varying amplitude is [20]:

$$\sigma_\mathrm{ab} = \alpha \frac{\delta - i\Gamma_\mathrm{bc}}{\delta^2 + (\Delta - i\gamma_\mathrm{ab} - i\Gamma_\mathrm{bc})\,\delta - |\Omega|^2 - i\Delta\Gamma_\mathrm{bc} - \gamma_\mathrm{ab}\Gamma_\mathrm{bc}}, \tag{2.1}$$

where $\delta = \omega_\mathrm{cb} + \omega_\mathrm{c} - \omega_\mathrm{p}$, γ_ab and Γ_bc are dephasing rates for the $|a\rangle \rightarrow |b\rangle$ and $|b\rangle \rightarrow |c\rangle$ transitions respectively.

The atomic response defined by Eq. (2.1) as a function of complex variable δ has two poles:

$$\delta_\pm = \frac{1}{2}\left(-\Delta + i\gamma_\mathrm{ab} + i\Gamma_\mathrm{bc} \pm \sqrt{4\,|\Omega|^2 + (\Delta - i\gamma_\mathrm{ab} + i\Gamma_\mathrm{bc})^2}\right). \tag{2.2}$$

These poles produce the resonant contributions to the atomic response and hence can be attributed to the effective states with frequencies and dephasing rates defined by the real and imaginary parts of $\delta_{\pm}$, respectively. In terms of these effective states, a slow-varying amplitude σ_{ab} can be presented as a superposition of two resonant responses associated with the transitions from the ground state to the corresponding decaying-dressed states:

$$\sigma_{\mathrm{ab}} = \frac{\alpha A_{+}}{(\delta - \delta_{+})} + \frac{\alpha A_{-}}{(\delta - \delta_{-})}, \tag{2.3}$$

where $A_{\pm}$ are defined as follows:

$$A_{\pm} = \pm \frac{\delta_{\pm} - i\Gamma_{\mathrm{bc}}}{\delta_{+} - \delta_{-}} = \pm \frac{\left(-\Delta + i\gamma_{\mathrm{ab}} - i\Gamma_{\mathrm{bc}} \pm \sqrt{\left(\Delta - i\gamma_{\mathrm{ab}} + i\Gamma_{\mathrm{bc}}\right)^{2} + 4\left|\Omega\right|^{2}} \right)}{2\sqrt{\left(\Delta - i\gamma_{\mathrm{ab}} + i\Gamma_{\mathrm{bc}}\right)^{2} + 4\left|\Omega\right|^{2}}}. \tag{2.4}$$

Let us note that exactly the same states define the behavior of two-photon coherence

$$\sigma_{\mathrm{bc}} = \frac{\alpha^{*} B_{+}}{(\delta - \delta_{+})} + \frac{\alpha^{*} B_{-}}{(\delta - \delta_{-})}, \tag{2.5}$$

where

$$B_{\pm} = \pm \frac{\Omega}{\delta_{+} - \delta_{-}} = \pm \frac{\Omega}{\sqrt{\left(\Delta - i\gamma_{\mathrm{ab}} + i\Gamma_{\mathrm{bc}}\right)^{2} + 4\left|\Omega\right|^{2}}}. \tag{2.6}$$

According to Eq. (2.2), $\mathrm{Re}\left(\delta_{+}\right)$ and $\mathrm{Re}\left(\delta_{-}\right)$ are equal to the level shifts of usual dressed states (i.e. the eigenvalues of the "atom+field" Hamiltonian) either when $\Gamma_{\mathrm{bc}} = \gamma_{\mathrm{ab}}$ or when $2\left|\Omega\right| \gg \max\{\left|\gamma_{\mathrm{ab}} - \Gamma_{\mathrm{bc}}\right|, \Delta\}$. Both quantities $\mathrm{Im}\left(\delta_{+}\right)$ and $\mathrm{Im}\left(\delta_{-}\right)$ in this case are equal to the sum of the dephasing rates regardless of the effective state involved. However, when dephasing rates Γ_{bc} and γ_{ab} are not equal $\Gamma_{\mathrm{bc}} \neq \gamma_{\mathrm{ab}}$, and their difference is non-negligible as compared to the Rabi frequency of the driving field, $\mathrm{Re}\left(\delta_{+}\right)$ and $\mathrm{Re}\left(\delta_{-}\right)$ are essentially different from the level shifts expected for the usual dressed states. In addition, the dephasing rates $\mathrm{Im}\left(\delta_{+}\right)$ and $\mathrm{Im}\left(\delta_{-}\right)$ characterizing the width of the corresponding resonant contributions become

very different from each other as well. These are the decaying-dressed states (but not the usual dressed states) which determine two effective resonant contributions to the atomic response when dephasing rates are essentially different. Hence the analysis based on decaying-dressed states allows for simple description and interpretation of various peculiarities of the total atomic response with change of the parameters as it will be demonstrated below.

C. Resonant driving

In the case of resonant driving, $\Delta = 0$, both the amplitudes and positions of resonances depend on a single parameter, which is different for the amplitudes and the positions. Namely, the amplitudes are defined by $x = 0.5\left(\gamma_{ab} - \Gamma_{bc}\right)/\left|\Omega\right|$, and the positions are defined by $y = 2\sqrt{\left|\Omega\right|^2 + \gamma_{ab}\Gamma_{bc}}/\left(\gamma_{ab} + \Gamma_{bc}\right)$. In terms of these parameters, the following expressions can be written:

$$A_{\pm} = 0.5 \pm i\frac{x}{2\sqrt{1-x^2}} \tag{2.7a}$$

and

$$\delta_{\pm} = 0.5\left(\gamma_{ab} + \Gamma_{bc}\right)\left(i \pm \sqrt{y^2 - 1}\right). \tag{2.7b}$$

Figures 3 and 4 present the dependence of A_+ and A_- on the parameter x, correspondingly. The analysis of these figures reveals three regions of distinctly different behavior: $x < -1$, $-1 < x < 1$, $x > 1$, and two bifurcation points $|x| = 1$. Comparison of these figures shows that changing $x \to -x$ corresponds to exchange of A_+ with A_- and vice versa.

Figures 5 and 6 present the dependence of $\mathrm{Re}\left(\delta_{\pm}\right)$ and $\mathrm{Im}\left(\delta_{\pm}\right)$ on the parameter y, correspondingly. The analysis of these figures reveals two regions of distinctly different behavior: $0 < y < 1$, $y > 1$ and a bifurcation point $y = 1$.

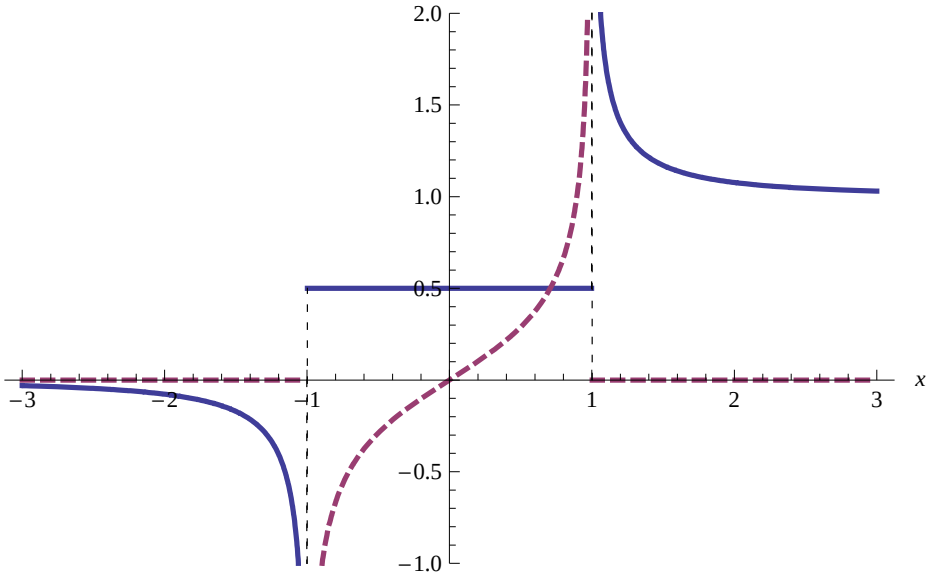

FIG. 3. Dependence of the real (solid line) and imaginary (dashed line) part of A_+ as a function of dimensionless parameter x defined in text.

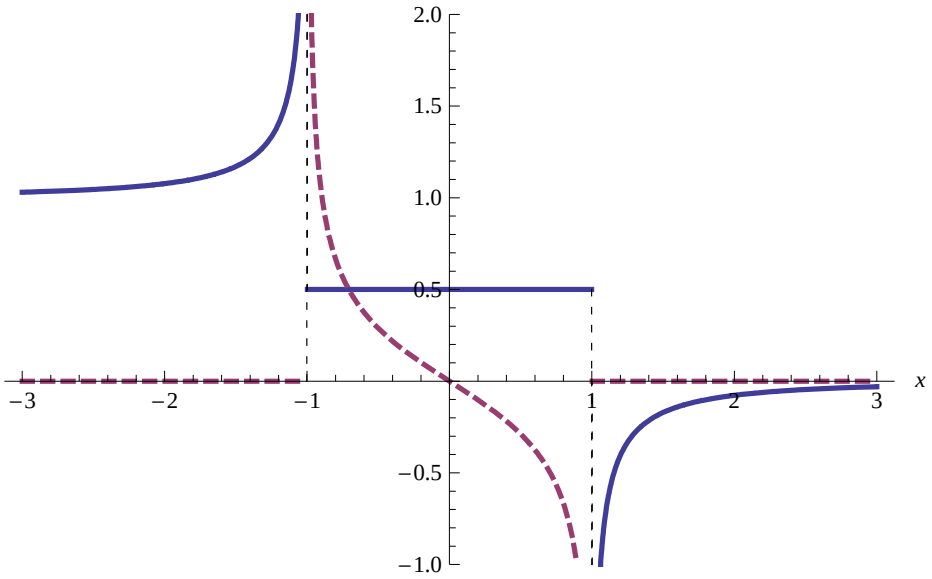

FIG. 4. Dependence of the real (solid line) and imaginary (dashed line) part of A_- as a function of dimensionless parameter x defined in text.

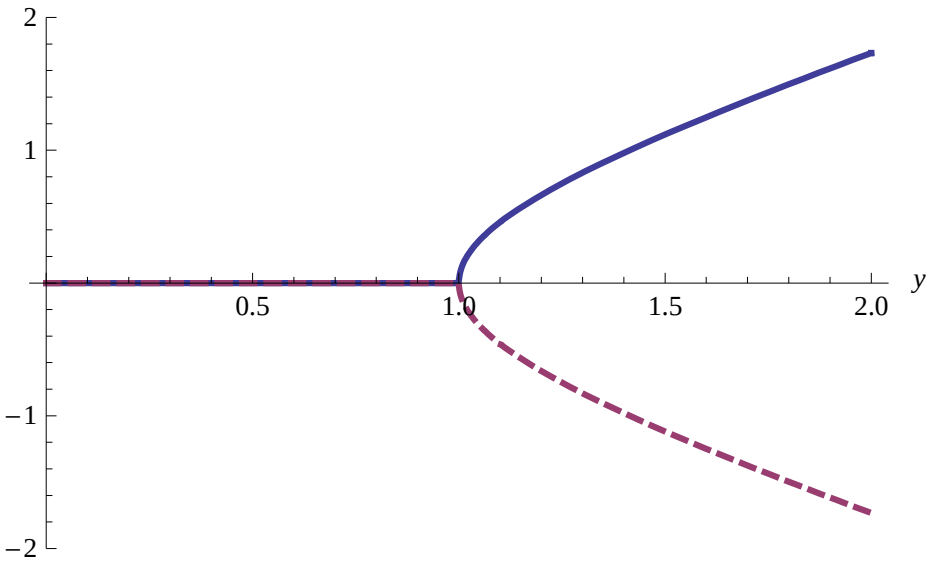

FIG. 5. Dependence of $2\mathrm{Re}\,(\delta_+)\,/\,(\gamma_{ab}+\Gamma_{bc})$ and $2\mathrm{Re}\,(\delta_-)\,/\,(\gamma_{ab}+\Gamma_{bc})$ as a function of dimensionless parameter y (see text for definition) is presented by solid and dashed line, respectively.

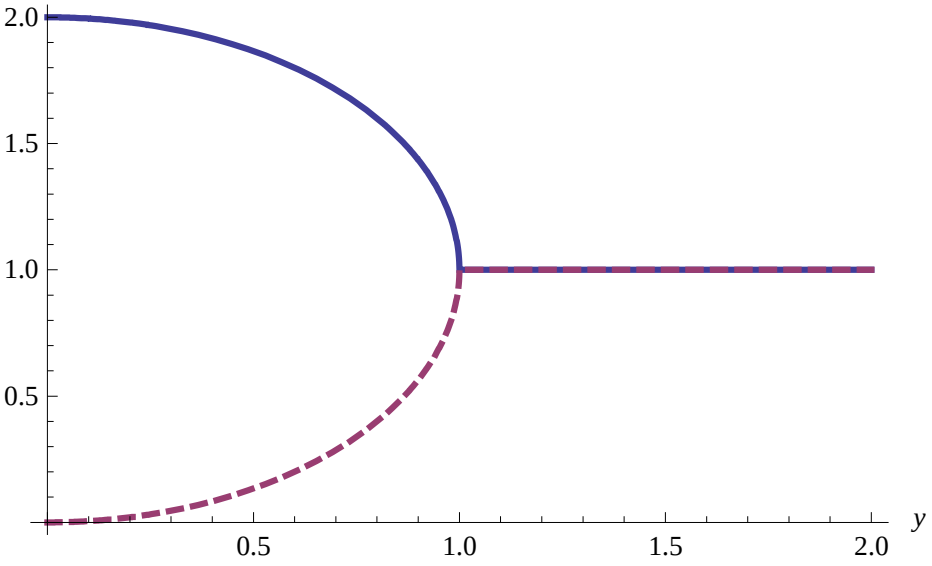

FIG. 6. Dependence of $2\mathrm{Im}\,(\delta_+)\,/\,(\gamma_{ab}+\Gamma_{bc})$ and $2\mathrm{Im}\,(\delta_-)\,/\,(\gamma_{ab}+\Gamma_{bc})$ as a function of dimensionless parameter y (see text for definition) is presented by solid and dashed line, respectively.

The relationship between the parameters x and y is given by the following:

- if $|x| > 1$ then $0 < y < 1$;
- if $|x| = 1$ then $y = 1$;
- if $|x| < 1$ then $y > 1$.

1. Weak resonant driving field, $|x| > 1$

The condition $|x| > 1$ implies either $x > 1$ or $x < -1$. The first possibility means that the two-photon coherence lives longer than the optical coherence while the second possibility means that the opposite is true. Careful examination shows that, although $A_{\pm}$ and $\delta_{\pm}$ are significantly affected by the choice of the sign of x, it is always possible to define $|1ph\rangle$ - the effective level which is mostly $|a\rangle$ and $|2ph\rangle$ - the effective level which is mostly $|c\rangle$. Transition from the ground level $|b\rangle$ to $|1ph\rangle$ ($|2ph\rangle$) is the one-photon (two-photon) transition.

The main signature of the one-photon transition is its presence in the absence of the driving field while the signature of the two-photon transition is its appearance if the driving field is applied. It can be seen from Figs. 3 and 4 that, for $x > 1$, $|+\rangle$ represents the one-photon transition while $|-\rangle$ represents a two-photon one. In the opposite case of $x < -1$ the role of $|+\rangle$ and $|-\rangle$ is exchanged. The dependence of the amplitudes on the strength of the driving field in the case $|x| \gg 1$ is the following:

$$A_{1ph} = 1 + |\Omega|^2 / (\gamma_{\mathrm{ab}} - \Gamma_{\mathrm{bc}})^2 , \tag{2.8a}$$

$$A_{2ph} = -|\Omega|^2 / (\gamma_{\mathrm{ab}} - \Gamma_{\mathrm{bc}})^2 . \tag{2.8b}$$

These dependences support the one-photon and two-photon assignments. The amplitude of the one-photon transition is real and always grater than one. This reflects

expected absorption from the ground state. The interesting feature of the two-photon transition is the negative value of its amplitude. This fact means that the two-photon transition provides gain in a three-level Λ system. Equation (2.8b) states that the gain increases with increasing of the driving field. The competition between the one-photon absorption and the two-photon gain depends dramatically on the dephasing rates γ_{ab} and Γ_{bc}. Thus the choice of positive or negative x affects greatly the profile of the atomic response and will be discussed later.

The real parts of the poles describe the positions of the decaying dressed states. In the case of a weak driving considered here, $\mathrm{Re}\,(\delta_{\pm}) = 0$ which is demonstrated by the region $0 < y < 1$ on Fig. 5. Hence, both resonances are centered at $|a\rangle \rightarrow |b\rangle$ transition instead of being split by $2\,|\Omega|$ as it could be expected on the basis of the usual dressed state picture. In turn, the imaginary parts of the poles describe the widths of the resonances, i.e. the dephasing rates of the transitions from the ground level to the corresponding decaying dressed state.

In the limit $|x| \gg 1$, the poles according to Eq. (2.7b) are defined as:

$$\delta_{1ph} = i\left(\gamma_{\mathrm{ab}} - |\Omega|^2 / \left(\gamma_{\mathrm{ab}} - \Gamma_{\mathrm{bc}}\right)\right), \tag{2.9a}$$

and

$$\delta_{2ph} = i\left(\Gamma_{\mathrm{bc}} + |\Omega|^2 / \left(\gamma_{\mathrm{ab}} - \Gamma_{\mathrm{bc}}\right)\right). \tag{2.9b}$$

In the absence of the driving field, the dephasing rate for the one-photon transition is equal to γ_{ab}, and for the two-photon transition coincides with Γ_{bc}. As one can see, the choice of which transition dephases faster affects mainly the width of the transition $2\mathrm{Im}\,(\delta_{1ph})$ $(2\mathrm{Im}\,(\delta_{2ph}))$ but not the amplitude A_{1ph} (A_{2ph}).

The dependence of the dephasing rates on the driving field is sensitive to the sign of x. This can be seen from Eqs. (2.9a) and (2.9b). Depending on $\gamma_{\mathrm{ab}} - \Gamma_{\mathrm{bc}}$,

the dephasing rate experiences power broadening or power narrowing. The narrowing (broadening) introduced to the one-photon transition becomes noticeable for $|\Omega|^2 \approx \gamma_{\rm ab}\,|\gamma_{\rm ab} - \Gamma_{\rm bc}|$ while for the two-photon transition it becomes noticeable for $|\Omega|^2 \approx \Gamma_{\rm bc}\,|\gamma_{\rm ab} - \Gamma_{\rm bc}|$. Comparison of these two cases shows that the narrower transition is affected by the presence of the driving field faster. The presence of the driving field always results in the broadening of the narrower resonance and the narrowing of the broad. This general tendency of the driving field to make the dephasing rates equal is supported by Eq. (2.7b), which shows dependence on y only. Finally, this tendency is demonstrated on Fig. 6 in $0 < y < 1$ region.

The profile of the atomic response is substantially different for $x > 1$ or $x < -1$. The case $x > 1$ corresponds to the broad one-photon absorption and the narrow two-photon amplification resonances both centered at $|b\rangle \rightarrow |a\rangle$ transition (see Fig. 7 top row). Combination of this two resonances results in a narrow dip at the center of the absorption profile. The width and the depth of the dip is defined by δ_{2ph} and A_{2ph}. It is remarkable that the amplification originated from the two-photon feature can be comparable to the one-photon absorption which leads to the net transparency at the center of the line. Indeed, the resulting value of $\mathrm{Im}\,(\sigma_{\rm ab})$ at the center of the dip is

$$\begin{aligned}
\mathrm{Im}\,(\sigma_{\rm ab})_{\delta=0}\,/\alpha &= A_{1ph}/\mathrm{Im}\,(\delta_{1ph}) + A_{2ph}/\mathrm{Im}\,(\delta_{2ph}) \\
&= \frac{1 + |\Omega|^2\,/\,(\gamma_{\rm ab} - \Gamma_{\rm bc})^2}{\gamma_{\rm ab} - |\Omega|^2\,/\,(\gamma_{\rm ab} - \Gamma_{\rm bc})} - \frac{|\Omega|^2\,/\,(\gamma_{\rm ab} - \Gamma_{\rm bc})^2}{\Gamma_{\rm bc} + |\Omega|^2\,/\,(\gamma_{\rm ab} - \Gamma_{\rm bc})} \\
&= \frac{1}{\gamma_{\rm ab}}\left(1 - \frac{|\Omega|^2}{\gamma_{\rm ab}\Gamma_{\rm bc} + |\Omega|^2}\right) \\
&= \frac{1}{\gamma_{\rm ab}\left(1 + |\Omega|^2\,/(\gamma_{\rm ab}\Gamma_{\rm bc})\right)}.
\end{aligned} \tag{2.10}$$

According to Eq. (2.10), $|\Omega|^2 = \gamma_{\rm ab}\Gamma_{\rm bc}$ defines the characteristic strength of the driving field when the absorption at the center of the dip is two times smaller than in

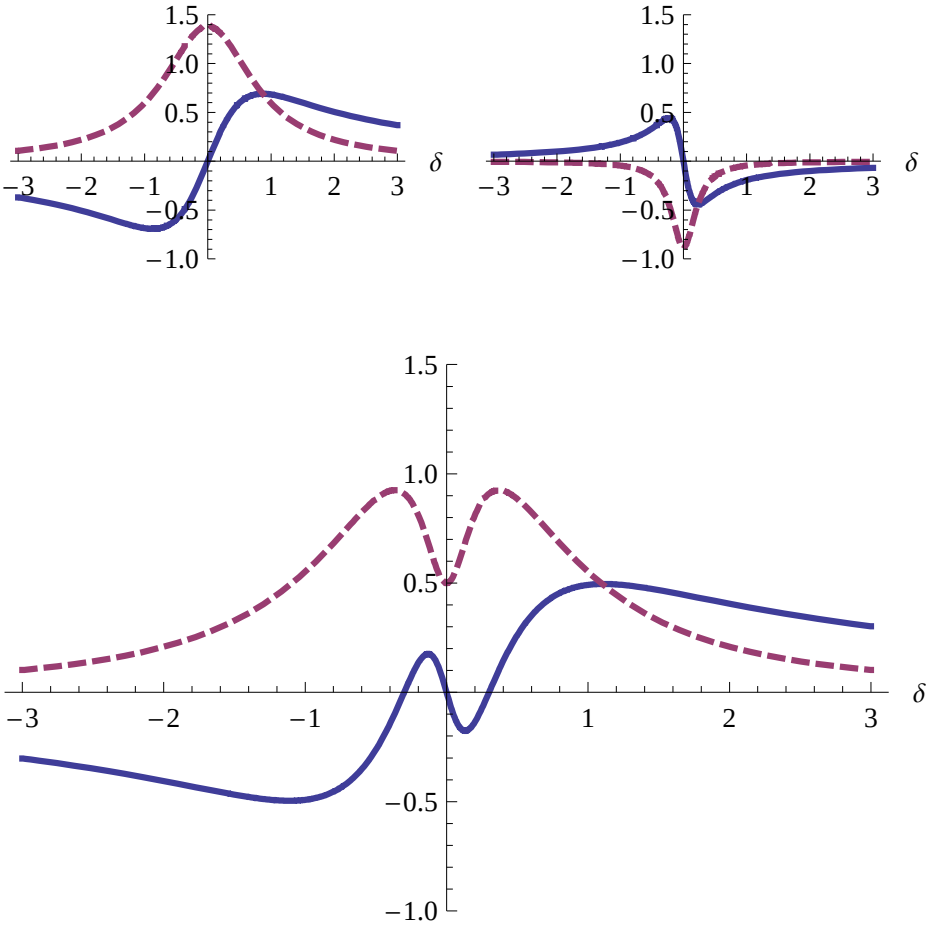

FIG. 7. The profile of the atomic response in the regime of electromagnetically induced transparency ($x = 2.84605$). (Top left) $\sigma_{\text{1ph-b}}$. (Top right) $\sigma_{\text{2ph-b}}$. (Bottom) Net response $\sigma_{\text{ab}} = \sigma_{\text{1ph-b}} + \sigma_{\text{2ph-b}}$. Real and imaginary parts are presented by the solid and dashed lines correspondingly. The numerical values for parameters used were the following: $\gamma_{\text{ab}} = 1$, $\Gamma_{\text{bc}} = 0.1$, $|\Omega|^2 = \gamma_{\text{ab}}\Gamma_{\text{bc}}$.

the absence of the driving field. (Note that the width of the two-photon resonance at this value of $|\Omega|$ remains quite narrow $\approx 2\Gamma_{\rm bc}$. With further increase of the driving field, the absorption at the center tends to zero.

In the finite range of the driving field intensities $\gamma_{\rm ab}\Gamma_{\rm bc} \leq |\Omega|^2 < (\gamma_{\rm ab} - \Gamma_{\rm bc})^2$, the sum of the broad absorption and narrow amplification profiles results in the characteristic feature of electromagnetically induced transparency (see Fig. 7). It has nothing to do with the Autler-Townes effect (dynamical Stark splitting of the atomic level in the presence of a strong field by 2Ω). Indeed, if one would formally consider the sum of two Lorentzians splitted by 2Ω with the effective width $(\gamma_{\rm ab} + \Gamma_{\rm bc})/2$ the absorption profile would be smooth with maximum in the center and small absorption deficit (as compared to the case of $\Omega = 0$) defined by the ratio $|\Omega|^2/\gamma_{\rm ab}^2$. In fact the non-absorbing feature originates from the difference of two Lorentzians centered at the same position, rather than summation of two Lorentzians shifted by the twice the Rabi frequency, which clearly reflects the importance of interference.

The case $x < -1$ corresponds to narrow absorption and broad amplification resonances. In the previous case ($x > 1$), the small gain present at the two-photon transition had a stronger impact on the profile of the atomic response. It was due to the fact that all gain was concentrated in a narrow region $\delta < \Gamma_{\rm bc} < \gamma_{\rm ab}$. However in the present case ($x < -1$), the gain is small and is spread over a much broader region $\gamma_{\rm ab} < \delta < \Gamma_{\rm bc}$. Therefore, the impact of the two-photon transition is greatly suppressed. For any $x < -1$, the summation of two resonances results in a smooth absorption profile with a maximum in the center (see Fig. 8 for the case of $x = -2.84605$) and small absorption deficit (as compared to the case of no driving field). Since $\Gamma_{\rm bc} > \gamma_{\rm ab}$ the condition $|\Omega|^2 \geq \gamma_{\rm ab}\Gamma_{\rm bc}$ implies $|\Omega| > \gamma_{\rm ab}$. Thus, it corresponds to the case of a strong driving field which is considered below.

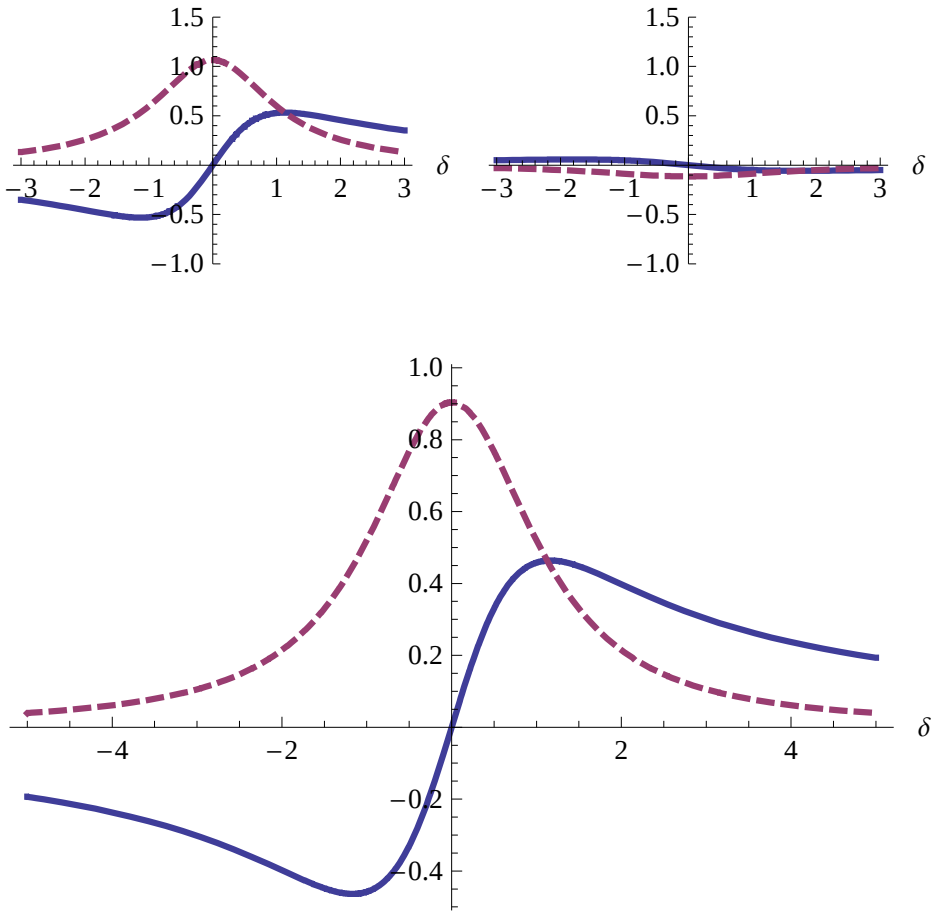

FIG. 8. The profile of the atomic response in the regime of electromagnetically induced transparency ($x = -2.84605$). (Top left) $\sigma_{\text{1ph-b}}$. (Top right) $\sigma_{\text{2ph-b}}$. (Bottom) Net response $\sigma_{\text{ab}} = \sigma_{\text{1ph-b}} + \sigma_{\text{2ph-b}}$. Real and imaginary parts are presented by the solid and dashed lines correspondingly. The numerical values for parameters used were the following: $\gamma_{\text{ab}} = 1$, $\Gamma_{\text{bc}} = 1.9$, $|\Omega|^2 = 0.1$.

2. Strong resonant driving field, $|x| < 1$

In the limit of a strong field, the transitions from the ground level to the decaying-dressed states can no longer be classified as one- or two-photon transitions. For the purpose of an illustration let us assume the limit $|x| \ll 1$. In this case,

$$A_{\pm} = \frac{1}{2} \pm i\frac{(\gamma_{\rm ab} - \Gamma_{\rm bc})}{4\,|\Omega|} \tag{2.11a}$$

and

$$\delta_{\pm} = \pm\left(|\Omega| - \frac{(\gamma_{\rm ab} - \Gamma_{\rm bc})^2}{8\,|\Omega|}\right) + i\frac{(\gamma_{\rm ab} + \Gamma_{\rm bc})}{2}. \tag{2.11b}$$

Thus, the amplitudes are real, positive quantities, which are equal to each other and equal to one half (except for a small imaginary correction which goes to zero with increase of the driving field). The dephasing rate for each transition is equal to an average dephasing rate $0.5\,(\gamma_{\rm ab} + \Gamma_{\rm bc})$, which does not depend on the driving field. Finally, the positions of decaying-dressed states essentially coincide with positions defined by the usual dressed states and are just slightly affected by the dephasing rates.

All the previous combined, the imaginary part of the atomic profile is represented by a sum of two Lorentzian profiles separated by the twice the Rabi frequency with the widths $(\gamma_{\rm ab} + \Gamma_{\rm bc})/2$. This corresponds to the ac-Stark splitting where the EIT feature is not present. It is worthwhile to point out that a strong field limit, $|x| < 1$, implies $|\Omega| > |\gamma_{\rm ab} - \Gamma_{\rm bc}|$ rather than $|\Omega| > \max\{\gamma_{\rm ab}, \Gamma_{\rm bc}\}$. At the same time, an observation of the resolved dynamic Stark splitting requires $|\Omega|^2 > 0.5\,(\gamma_{\rm ab}^2 + \Gamma_{\rm bc}^2)$. Thus in the case $\Gamma_{\rm bc} > \gamma_{\rm ab}$ it requires $|\Omega| > \Gamma_{\rm bc} > \gamma_{\rm ab}$ rather than just $|\Omega| > \gamma_{\rm ab}$.

3. Bifurcation points $x = 1$ and $x = -1$

A bifurcation point is a special case for which $|x| = 1$ and where the atomic response has a pole of the second order:

$$\sigma_{\mathrm{ab}} = \frac{\alpha\left(\delta - i\Gamma_{\mathrm{bc}}\right)}{\left(\delta - i\left(\gamma_{\mathrm{ab}} + \Gamma_{\mathrm{bc}}\right)/2\right)^2}, \tag{2.12}$$

In this degenerate case, the presentation of the atomic response as a superposition of two Lorentzians is no longer valid.

Figures 9 and 10 demonstrate the atomic response at the bifurcation point $x = 1$ and $x = -1$ respectively. Dip in the center is present for $x = 1$ and is absent for $x = -1$.

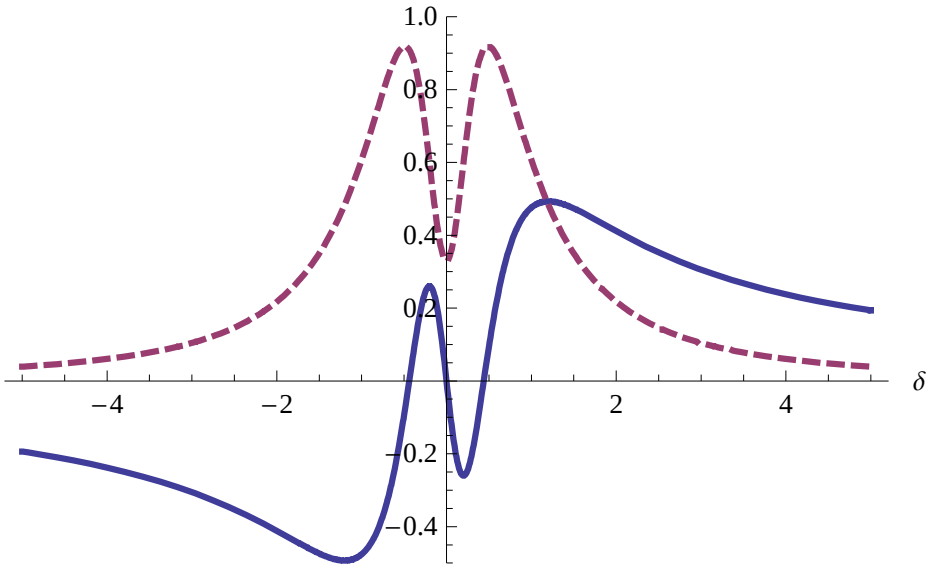

FIG. 9. Demonstration of the atomic response at the bifurcation point $x = 1$ where the behavior of the effective states changes. The following numerical parameters we used: $\gamma_{\mathrm{ab}} = 1$, $\Gamma_{\mathrm{bc}} = 0.1$ and $\Omega = 0.45$.

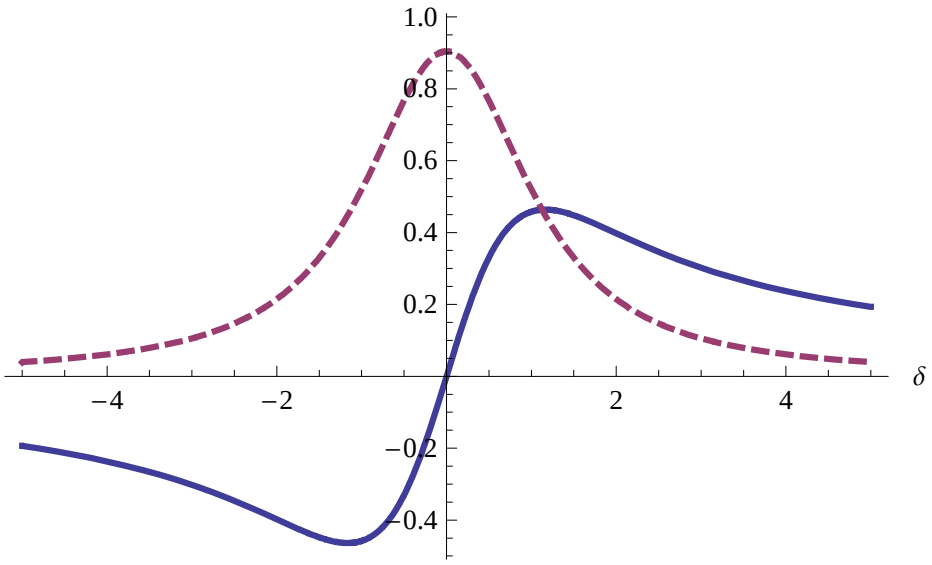

FIG. 10. Demonstration of the atomic response at the bifurcation point $x = -1$ where the behavior of the effective states changes. The following numerical parameters we used: $\gamma_{\rm ab} = 1$, $\Gamma_{\rm bc} = 1.9$ and $\Omega = 0.45$.

D. Weak far detuned driving field

In the case when a weak driving field is far detuned from the one-photon resonance, one can assume for all practical purposes that $\Delta - i\gamma_{\rm ab} + i\Gamma_{\rm bc} \approx \Delta$ and $\Delta \gg |\Omega|$. Under such assumptions the decaying-dressed states are represented by

$$A_{1ph} = 1 - \frac{|\Omega|^2}{\Delta^2}, \tag{2.13a}$$

$$\delta_{1ph} = -\Delta\left(1 + \frac{|\Omega|^2}{\Delta^2}\right) + i\gamma_{\rm ab}\left(1 - \frac{|\Omega|^2}{\Delta^2}\right), \tag{2.13b}$$

and

$$A_{2ph} = \frac{|\Omega|^2}{\Delta^2}, \tag{2.14a}$$

$$\delta_{2ph} = \frac{|\Omega|^2}{\Delta} + i\left(\Gamma_{\rm bc} + \frac{|\Omega|^2\gamma_{\rm ab}}{\Delta^2}\right). \tag{2.14b}$$

Here, the one- and two-photon nature of the resonances clearly appears again. The positions of the resonances ($\mathrm{Re}\,(\delta_{\pm})$) coincide with positions of the usual dressed states split by Δ. Therefore, two resonances in this case are well separated and never overlap. It makes sense to discuss the profile of atomic response for the one-photon transition independently from the two-photon transition.

1. One-photon transition

The atomic response for one-photon transition is equivalent to the atomic response of an effective two level system and is proportional to

$$\sigma_{-b} = \frac{1-\zeta}{\delta + \Delta\,(1+\zeta) - i\gamma_{\mathrm{ab}}\,(1-\zeta)}, \tag{2.15}$$

where $\zeta = |\Omega|^2/\Delta^2$ and is valid for $\zeta \ll 1$. It describes Lorentzian absorption profile centered at $\delta_0 = -\Delta\,(1+\xi)$. Thus, the center of the profile is slightly shifted up from $|a\rangle \rightarrow |b\rangle$ transition by the two-photon Rabi frequency $|\Omega|^2/\Delta$. The width of this resonance in the weak field is defined by γ_{ab}. Both the width and amplitude decrease with increase of the driving field in such a manner that the magnitude of the maximal absorption remains constant.

2. Two-photon transition

The $|b\rangle \rightarrow |+\rangle$ transition is a two-photon transition. Corresponding atomic response is fully defined by the presence of the driving field and is proportional to

$$\sigma_{+b} = \frac{\Gamma_{\mathrm{bc}}}{\gamma_{\mathrm{ab}}}\frac{\xi}{(\delta - \Gamma_{\mathrm{bc}}(\Delta/\gamma_{\mathrm{ab}})\xi - i(\xi+1)\Gamma_{\mathrm{bc}})}, \tag{2.16}$$

where $\xi = \gamma_{\mathrm{ab}}\zeta/\Gamma_{\mathrm{bc}}$, which can be greater than one if $\Gamma_{\mathrm{bc}} \ll \gamma_{\mathrm{ab}}$ even at $\zeta \ll 1$.

This atomic response corresponds to the absorption in an effective two-level system, which resonance frequency is shifted down from $|a\rangle \rightarrow |b\rangle$ transition by

$\Delta + |\Omega|^2/\Delta$. The last term can be presented also as $\Delta\xi\Gamma_{\rm bc}/\gamma_{\rm ab}$. At the first stage of increasing ξ, while $\xi < 1$, the width of the resonance is defined by $\Gamma_{\rm bc}$ (hence it may be much more narrow than the width of one-photon resonance) and the absorption is increasing linearly with ξ. When $\xi = 1$, the power broadening doubles the width of the resonance and $\mathrm{Im}\left(\sigma_{+b}\right)_{\max} = 0.5\gamma_{\rm ab}^{-1}$. It is half of the maximal value: $\mathrm{Im}\left(\sigma_{+b}\right)_{\max} = \gamma_{\rm ab}^{-1}$ which is reached when $\xi \to \infty$. Further increase in ξ leads to increase of the width of the resonance.

It is remarkable that strong response ($\mathrm{Im}\left(\sigma_{+b}\right)_{\max} = 0.5\gamma_{\rm ab}^{-1}$ - comparable to the resonant one-photon response in the absence of the driving field) can be achieved in the far-detuned ($\Delta \gg \gamma_{\rm ab}$ and $\Delta \gg |\Omega|$) three-level system at the two-photon transition under the condition $\xi \approx 1$ due to the slow dephasing of the two-photon coherence σ_{bc}.

E. Strong far detuned driving field

In the case of a strong far-detuned drive such that $\zeta \gg 1$. The atomic response is described by

$$A_{\pm} = \frac{1}{2} \mp \frac{\Delta - i\left(\gamma_{\rm ab} - \Gamma_{\rm bc}\right)}{4\left|\Omega\right|} \tag{2.17}$$

$$\delta_{\pm} = -\frac{\Delta}{2} \pm \left|\Omega\right| + \frac{i}{2}\left(\gamma_{\rm ab} + \Gamma_{\rm bc}\right) \pm \frac{\left(\Delta - i\left(\gamma_{\rm ab} - \Gamma_{\rm bc}\right)\right)^2}{8\left|\Omega\right|} \tag{2.18}$$

Thus the case of a strong far-detuned drive is equivalent to a strong resonant drive considered in Section 2.

F. Large decay rate at the two-photon transition

In the case of fast dephasing of two-photon coherence, $\Gamma_{\rm bc} \gg \max\{\Delta, \gamma_{\rm ab}, |\Omega|\}$, only one effective level contributes to the atomic response:

$$A_- = 1 \tag{2.19a}$$

and

$$\delta_- = -\Delta + i\gamma_{\rm ab} + i\frac{|\Omega|^2}{\Gamma_{\rm bc}} \tag{2.19b}$$

It means that only one-photon resonance is important for a probe field. Its position is defined by the usual dressed state ($\delta_- = -\Delta$) and its width is defined by dephasing of the corresponding one-photon transition $\gamma_{\rm ab}$ which is slightly power broadend by the driving field.

G. Conclusion

We discussed decaying dressed states of a coherently driven three-level system as the effective states providing resonant contributions to the total atomic response. The analysis of such contributions allows for simple and straightforward classification of different regimes. In the case of slow dephasing of two-photon coherence and sufficiently weak driving field the decaying dressed states are dramatically different from the eigenstates of the "atom+field" Hamiltonian and especially useful for understanding the structure of the atomic response and its modifications with the variation of the parameters. Using decaying dressed sates should be helful also for analysis of other schemes including strong driving field.

CHAPTER III

SUPPRESSION OF γ-PHOTON ABSORPTION VIA QUANTUM INTERFERENCE*

We show that the interference effects (similar to electromagnetically induced transparency, which was widely studied earlier at the electronic transitions in optics) may appear in γ-radiation at the nuclear transitions under the condition of the nuclear level anticrossing. We demonstrate it also experimentally in the optically thin samples of $FeCO_3$.

A. Introduction

The quantum interference effects (such as electromagnetically induced transparency (EIT), slow light, lasing without inversion, etc.) represent one of the most rapidly developing fields of research in quantum optics. These effects appear in the three-level quantum systems driven by the strong coherent field at one transition and probed by the weak field at the adjacent transition. In the particular case of two quantum states having the same energy, the transition between these degenerate levels can be efficiently driven by a dc-field. This situation can be realized, for example, under the condition of level anticrossing (i.e. level mixing) in the external magnetic field. Quantum interference effects were widely studied both theoretically and experimentally in the optical range of frequencies at the electronic transitions mainly in gaseous

*This is a pre-print version of "Suppression of γ-photon absorption via quantum interference" by Petr Anismov, Farit Vagizov, Yuri Rostovtsev, Rustem Shakhmuratov and Olga Kocharovskaya from Journal of Modern Optics (2007) Vol. 54 (16 & 17), pp. 2595 - 2605 [59]. Reprinted with permission by Taylor & Francis. http://www.informaworld.com

media [20, 24, 26, 27, 21, 28] and more recently in solids [29, 30, 31, 32, 33].

A few years ago a level mixing induced transparency (LMIT) was reported for the first time at the nuclear γ-ray transition [60]. A more detailed experimental and theoretical analysis of this effect was provided in the following papers [61, 62, 36, 63, 64, 65]. The experiments were done in a $FeCO_3$ crystal with an optical thickness for the resonant γ-quanta of the order of 10. About 25% suppression of the resonant γ-ray absorption in ^{57}Fe was observed under the condition of the nuclear level crossing. This effect was attributed to the multiple scattering with a polarization change in the optically thick sample [63, 64, 65]. Hence it should not appear in the thin samples.

In this paper we report an experimental demonstration of the level mixing induced transparency for γ-photons in the thin sample of $FeCO_3$ and show that this effect can be viewed as EIT for single γ-photons at the nuclear transitions.

B. The characteristics of the samples and the experimental results

We perform the Mössbauer experiments in the natural mineral siderite, $FeCO_3$. The nuclear spin of ^{57}Fe is equal to $I_g = 1/2$ in the ground state and to $I_e = 3/2$ in the excited (14.4 keV) state. The siderite does not have cubic symmetry thus it has an electric field gradient which interacts with the nucleus' quadrupole moment and splits the excited state by 23.84 MHz. At the temperature below the Néel temperature [$T_N = 38.3^\circ\ K$] (see Ref. [66]) siderite becomes anti-ferromagnetic with an internal magnetic field, B_0 being parallel or anti-parallel to the electric field gradient. This direction is naturally chosen as a quantization z-axis. Thus the Hamiltonian of the system has a form:

$$H = \begin{bmatrix} H_e & V_\gamma \\ (V_\gamma)^\dagger & H_g \end{bmatrix} \tag{3.1}$$

where H_e is a 4×4 Hamiltonian for an excited state manifold; H_g is a 2×2 Hamiltonian for a ground state manifold, and $V_\gamma = -\mu_\gamma \mathbf{B}_\gamma$ describes a magnetic dipole interaction with a probing γ-radiation, where μ_γ is a magnetic dipole moment of the transition, and $\mathbf{B}_\gamma$ is a magnetic field of a probing γ-radiation.

The Hamiltonian for an excited state manifold includes magnetic and quadrupole contributions $H_e = H_Z + H_Q$ which are in turn

$$H_Z = -\gamma_e \left(\mathbf{I}_e\right)_z B_0 \tag{3.2}$$

and

$$H_Q = V_q \left(3 \left(\mathbf{I}_e\right)_z^2 - I_e \left(I_e + 1\right)\right), \tag{3.3}$$

where γ_e is the gyromagnetic ratio for an excited state. While the Hamiltonian for a ground state manifold includes only magnetic contribution $H_g = -\gamma_g \left(\mathbf{I}_g\right)_z B_0$, where γ_g is the gyromagnetic ratio for a ground state. $V_q = eQV_{zz}/\left(4I\left(2I-1\right)\right)$, where Q is the nuclear quadrupole moment, and V_{zz} is zz-component of the electrostatic gradient tensor.

The structure of the energy levels is given in Fig. 11. In the crystal sample the transition probability depends on the geometry of the experiment. If a probe γ-radiation propagates along z-axis, the transitions with $\Delta m = +1$ (corresponding to the lines 1 and 5 in Fig. 11 and described by $V_\gamma^+ = -\mu^+ \left(\left(\mathbf{B}_\gamma\right)_x + i \left(\mathbf{B}_\gamma\right)_y\right)$) and with $\Delta m = -1$ (corresponding to the lines 3 and 4 and described by $V_\gamma^- = -\mu^- \left(\left(\mathbf{B}_\gamma\right)_x - i \left(\mathbf{B}_\gamma\right)_y\right)$) are allowed. In the case when a probe γ-radiation propagates in the direction perpendicular to z-axis the transitions with $\Delta m = 0$ (lines 2 and 6; $V_\gamma^0 = -\mu^0 \left(\mathbf{B}_\gamma\right)_z$) also become possible. Because of equal populations in the ground state and a fundamental chiral symmetry of electromagnetic interaction the transitions $m \to m'$ should be identical to the transitions $-m \to -m'$ (corresponding

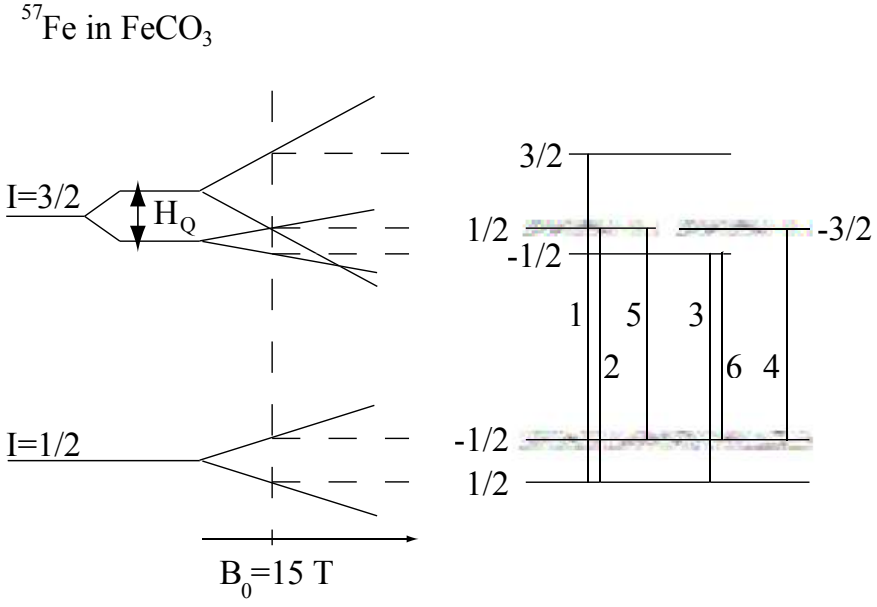

FIG. 11. Level diagram and possible transitions in siderite. Energy levels, we are focused on, are shaded.

to the reverse direction of z axis). Thus, for a single crystal sample depending on a geometry of the experiment the Mössbauer absorption spectra should consist of either two (1-4 and 3-5) or three doublets (1-4, 3-5 and 2-6) with identical lines (i.e. the same shape, width and amplitudes) in each doublet.

At T=30° K, when the internal magnetic field B_0 is approximately 15 T, Zeeman sublevels $-3/2$ and $1/2$ should cross each other and therefore two lines 4 and 5 should merge into one line. Thus, in the optically thin sample an absorption of the merging line should be equal to the sum of the absorption of lines 4 and 5, which in turn is equal to the sum of 1 and 3 absorption lines.

On the other hand, in an optically thick sample one could expect that an increase of the optical thickness of merging line to lead to summation of the absorption coefficients in the exponent rather than to summation of two exponents with original

absorption coefficients. It would result in absorption saturation of lines 4 and 5 at their crossing point as compared to the sum of absorption of their partner's lines 1 and 3 at the exit of the absorbing medium. However such a simple "thickness" argument does not hold in the case of a parallel geometry.

Indeed, the radioactive source in both our and the previous experiments was unpolarized and thus could be thought of as emitting γ-photons of a right and left circular polarizations one by one following each other with an equal probability. In a parallel geometry each of these photons may excite only one corresponding transition: either $\Delta m = +1$ (line 5) or $\Delta m = -1$ (line 4) depending on the polarization of the coming photon. Thus the total absorption of the merging lines should be determined by the sum of 1 and 3 absorption lines at the exit of the sample independent on its thickness. However, the earlier experiments in the optically thick samples with an optical thickness for the resonant γ-quanta of an order of 10 done at the Catholic Leuven University had shown that an absorption at the level crossing was about 25% smaller than the sum of absorptions at 1 and 3 lines independent on the geometry.

It is important to note that we repeated the same experiment at Texas A&M University with a crystal sample with an optical thickness of 7 for the resonant γ-quanta[3] in a parallel geometry and received a similar result (see Fig. 12). Such a deficit in absorption at the level crossing point was interpreted via the scattering of γ-photons with a polarization change in the optically thick crystal sample with a broken axial symmetry [63, 64, 65]. If this scattering process and the simple thickness effect would be the only mechanisms for the observed transparency, the transparency

[3]The reason for the high transparency is the following. The recoilless fraction of radiation both in the emitter and absorber is only about 70% while our detector registers both resonant and off-resonant gamma-quanta. Besides, emitted radiation is not polarized, while absorption of each resonant line is specified for radiation with particular polarization, left or right circularly polarized.

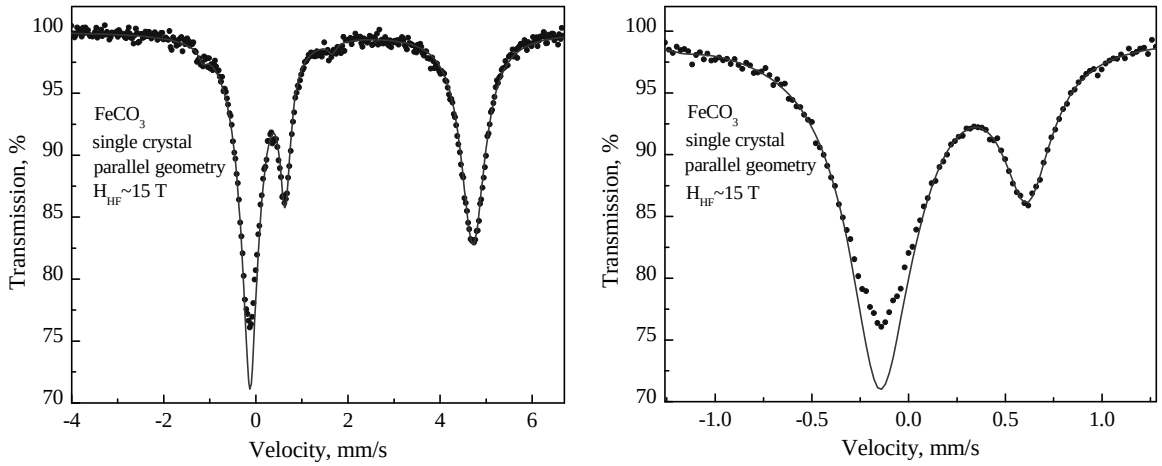

FIG. 12. Transmission spectrum of a single crystal sample (left). The $FeCO_3$ single crystal sample is cleaved and polished on both sides; it is a 60-70 μm thick platelet of 0.8x0.7 cm^2 area. The angle of the c-axis with the cleavage plane $\{10\bar{1}1\}$ is about $\pi/4$, and γ-ray wave vector is along the c-axis. This platelet is pasted up on a thin 1.1 mm copper plate with γ-ray aperture of 6 mm in diameter. The copper plate is screwed on a cold finger of the He closed cycle cryostat from Cryo Industries. Sample's optical thickness for the resonant γ-quanta is about 7. Zoom in at the level crossing is shown on the right.

should vanish in the optically thin sample.

We did the further Mössbauer experiments with the poly-crystal powder for two reasons. First, it is technically easier to prepare optically thin powder samples. Second, the scattering mechanism discussed in Ref. [63, 64] should be eliminated in a powder sample where the orientation of the optical axis is random and hence all three doublets are present in the spectrum. The experiments were performed by using a conventional Mössbauer set up. It includes a source of γ-radiation (Co^{57} in Rhodium), an absorber ($FeCO_3$ in powder), and a detector. The results for different optical thicknesses of an absorber are presented in Fig. 13. It clearly shows that

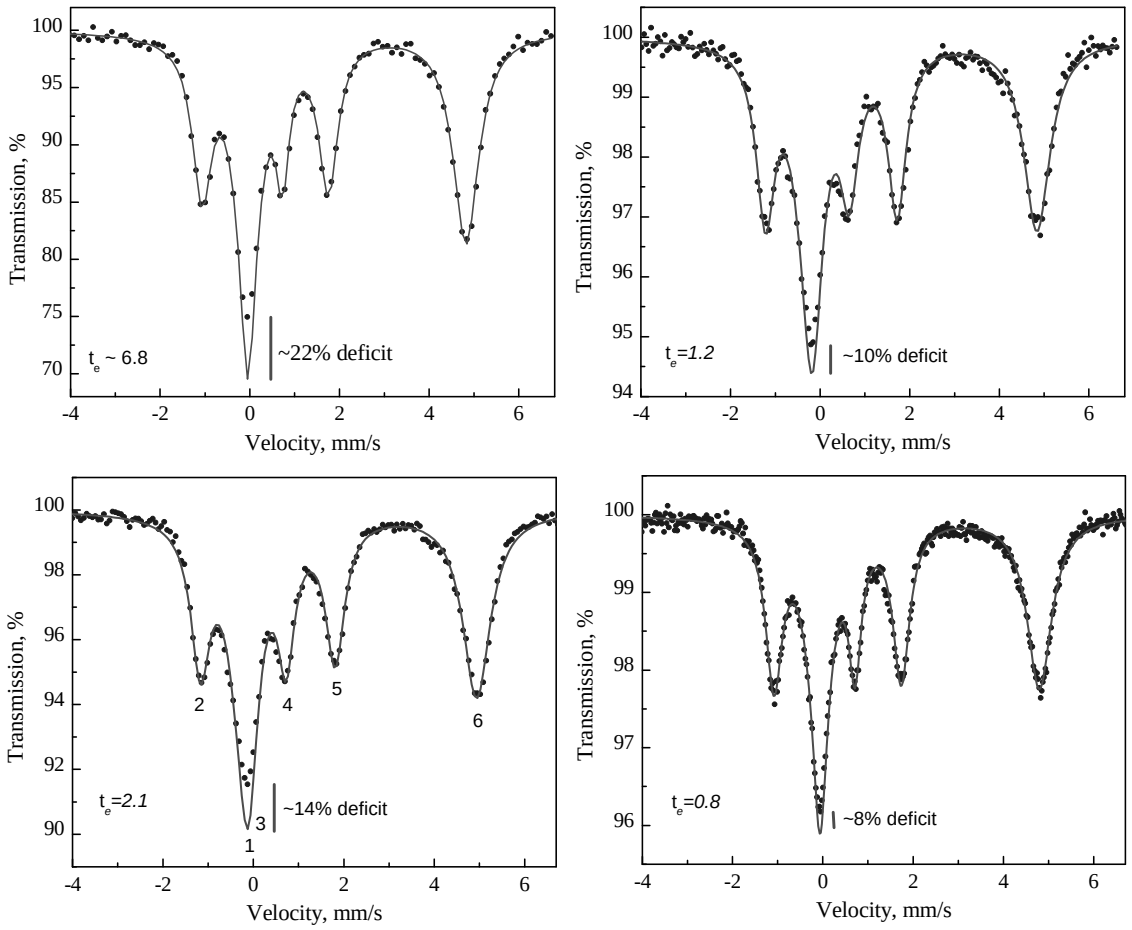

FIG. 13. Transmission spectra of ^{57}Fe:$FeCO_3$ powder samples for different optical thicknesses (t_e) of an absorber. Dots are the observed absorption while solid lines are the fitting curves based on the assumption that absorption at a merging line is equal to the sum of individual absorptions. Samples were cooled down to 30° K.

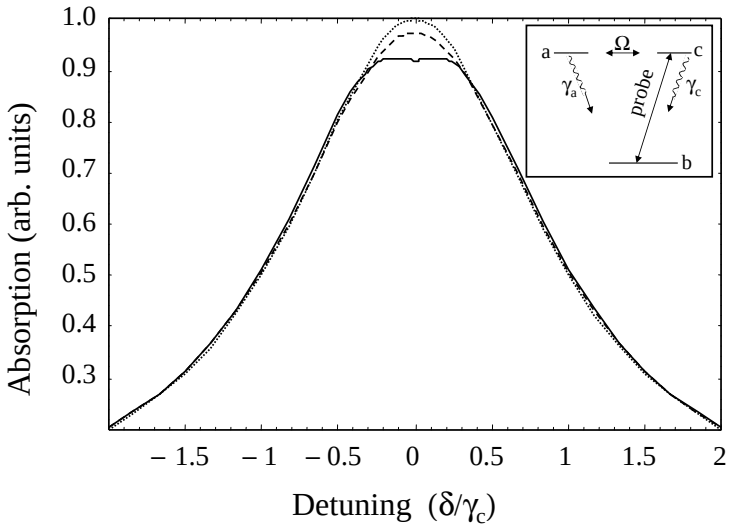

FIG. 14. Absorption curves for V_0^- probing γ-radiation. (i) dotted line corresponds to $\Omega = 0$, $\gamma_c = 1$, and $\gamma_a = 0.31$; (ii) solid line corresponds to $\Omega = 0.1644\gamma_c$, $\gamma_c = 1$, and $\gamma_a = 0.31$; (iii) dashed line corresponds to $\Omega = 0.1644\gamma_c$, $\gamma_c = 1$, and $\gamma_a = 1$

transparency is reduced with a decrease of the sample thickness. At the same time an appreciable deficit in absorption (about 8%) appears even in the sample with an optical thickness for the resonant γ-quanta equal to 0.8.

In the next section we provide a theoretical analysis of the level crossing transparency effect in thin samples. We show that the mechanism of LMIT in thin samples is essentially the same as EIT which was widely studied at the electronic optical transitions.

C. Mechanism of LMIT in thin samples

In order to understand the origin of the absorption deficit at the level crossing condition we consider a simplified three-level system involving only sublevels of interest. Namely, these are $m = 1/2$ and $m = -3/2$ sublevels, which are crossing in the excited

state, and a single $m = -1/2$ sublevel in the ground state. Let us denote them a, c, and b accordingly (Fig. 14). Similar to previous papers [60, 61, 62, 36, 63, 64, 65] we suppose that the axial symmetry is broken. (It may be caused by the presence of either perpendicular components of the internal magnetic field or asymmetry of the electric field gradient.) Breaking of the axial symmetry means coupling between the two degenerated upper levels a and c. Such a coupling results in the nuclear responses to probe γ-radiation simultaneously at $c-b$ and $a-b$ transitions. Their interference under certain conditions may lead to the reduced absorption. Indeed, when the axial symmetry is broken, the effective Hamiltonian of the system takes the form ($\hbar = 1$):

$$H^{eff} = \begin{array}{c} \\ a \\ b \\ c \end{array} \begin{array}{c} \begin{array}{ccc} a & b & c \end{array} \\ \begin{bmatrix} \omega_a & V^+ & \Omega \\ V^+ & 0 & V^- \\ \Omega & V^- & \omega_a \end{bmatrix} \end{array} \tag{3.4}$$

where Ω is a coupling due to the broken axial symmetry. Assuming that γ-radiation interacts with both $\Delta m = -1$ and $\Delta m = +1$ transitions and taking into account that it is weak and does not perturb the populations (i.e. $\rho_{bb} = 1$, $\rho_{aa} = \rho_{cc} = 0$), we obtain in the rotation wave approximation the following equations for the off-diagonal matrix elements at the probed transitions :

$$\frac{\partial \rho_{ab}}{\partial t} = -\left(\gamma_a + i\delta\right)\rho_{ab} - i\left(V_0^+ + \Omega\rho_{cb}\right), \tag{3.5}$$

$$\frac{\partial \rho_{cb}}{\partial t} = -\left(\gamma_c + i\delta\right)\rho_{cb} - i\left(V_0^- + \Omega\rho_{ab}\right), \tag{3.6}$$

where γ_a and γ_c are decay constants for the off-diagonal density matrix elements, and δ is the detuning from the transition frequency [67].

To get a deeper insight into the physics of LMIT we consider first the case when the probe field interacts only with the $\Delta m = -1$ transition (i.e. $V_0^+ = 0$). Then we

come to the so called Λ scheme. The steady-state solution of the above equations takes the form:

$$\rho_{ab} = -\frac{\Omega}{(\gamma_a + i\delta)} \frac{V_0^-}{\left(\gamma_c + i\delta + |\Omega|^2 / (\gamma_a + i\delta)\right)}, \tag{3.7}$$

and

$$\rho_{cb} = -i \frac{V_0^-}{\gamma_c + i\delta + |\Omega|^2 / (\gamma_a + i\delta)}. \tag{3.8}$$

Hence the susceptibility of the system is defined as:

$$\chi \sim -i \frac{|\mu^-|^2}{\gamma_c + i\delta + |\Omega|^2 / (\gamma_a + i\delta)} \tag{3.9}$$

or

$$\chi \sim -i \frac{|\mu^-|^2}{2} \left(\frac{1+A}{B_+ + i\delta} + \frac{1-A}{B_- + i\delta} \right) \tag{3.10}$$

where

$$A = \frac{\gamma_c - \gamma_a}{\sqrt{(\gamma_c - \gamma_a)^2 - 4\Omega^2}}, \tag{3.11}$$

and

$$B_\pm = \frac{\gamma_a + \gamma_c}{2} \pm i \sqrt{\Omega^2 - \left(\frac{\gamma_c - \gamma_a}{2} \right)^2}. \tag{3.12}$$

If the linewidths of both $a-b$ and $c-b$ transitions were equal to each other ($\gamma_a = \gamma_c$), then for arbitrary coupling between the excited states the total line shape (Eq. 3.10) presents the sum of two Lorentzians with centers separated by a coupling constant 2Ω and identical linewidths and amplitudes. This result has a transparent interpretation in the basis of the states dressed by Ω. Namely, it means that the total line results from the summation of the dressed level lines separated by 2Ω at the crossing point (level anti-crossing), and interference effects (associated with a contribution of the coherence between the dressed states) do not play any role. This effect is also well-known as the Autler-Townes effect (i.e. probing by γ-radiation of the Stark splitting produced by Ω). If the linewidths at $a-b$ and $c-b$ transitions in our Mössbauer

experiments were defined by the radiative decay, they would be equal to each other. Hence the absorption deficit (if any) in this case could be caused only by the level splitting and nuclear interference would not appear.

However, as it is clearly seen from the experimental data (see Fig. 12), the linewidths for these transitions are different, namely, $\Delta\omega_{\pm 3/2} = 0.592$ mm/s and $\Delta\omega_{\pm 1/2} = 0.260$ mm/s. In this case the total line shape (Eq. 3.10) cannot be viewed as a sum of two Lorentzians produced by the dressed states, and the interference effects play a crucial role. Let us consider the case when $\gamma_c > \gamma_a$ (which corresponds to our experimental scheme). According to (Eqs. 3.10-3.12), in the weak coupling case, namely $\Omega \ll (\gamma_c - \gamma_a)/2$, the total linewidth represents itself as the difference of two Lorentzians both centered at the merging lines frequency. The positive Lorentzian has a broad linewidth defined as $\gamma_c - \Omega^2/(\gamma_c - \gamma_a)$ (which is reduced with an increase of Ω) and a negative Lorentzian has a narrower linewidth $\gamma_a + \Omega^2/(\gamma_c - \gamma_a)$ which is power broadened. The absorption coefficient in the crossing point is proportional to $(\gamma_c + \Omega^2/\gamma_a)^{-1}$. Thus an absorption deficit due to the coupling is proportional to $\Omega^2/(\gamma_c\gamma_a)$. Note that the deficit in absorption for a given γ_c in the case $\gamma_a < \gamma_c$ is larger than in the case $\gamma_a = \gamma_c$. This means that an interference in absorption is destructive (coherence between the dressed states reduces the absorption).

According to our experimental data, the linewidth at $c-b$ transition is about two times broader than the linewidth at $a - b$ transition (see Fig. 12). (It is worthwhile to point out that this fact was noticed earlier and connected to the broadening of $1/2 \rightarrow -3/2$ line by coupling of the nuclear spin to the fast fluctuating electronic spin [66, 68]). This experimentally measured linewidth results from a convolution of both the radiative source and absorber lines. Taking into account that the linewidth of our source is known to be equal to 0.11 mm/s we conclude that $\gamma_c/\gamma_a \approx 3.217$.

The absorption curves for V_0^- probing γ-radiation corresponding to the cases (i)

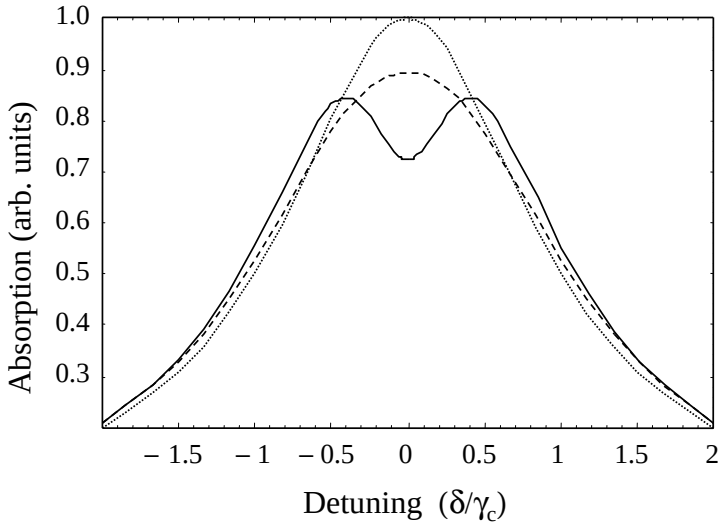

FIG. 15. Absorption curves for V_0^- probing γ-radiation in the case of a strong coupling. (i) dotted line corresponds to $\Omega = 0$, $\gamma_c = 1$, and $\gamma_a = 0.31$; (ii) solid line corresponds to $\Omega = (\gamma_c - \gamma_a)/2 = 0.345$, $\gamma_c = 1$, and $\gamma_a = 0.31$; (iii) dashed line corresponds to $\Omega = 0.345$, $\gamma_c = 1$, and $\gamma_a = 1$

$\Omega = 0$ and (ii) $\Omega = 0.1644\gamma_c$ for $\gamma_c/\gamma_a = 3.217$ are shown in Fig. 14. As it can be seen from the figure the absorption deficit is about 8%. The case (iii) $\Omega = 0.1644\gamma_c$ and $\gamma_a = \gamma_c$ is also presented for comparison. Note again that the deficit in absorption is larger in the case of $\gamma_c/\gamma_a = 3.217$ than it would be in the case $\gamma_a = \gamma_c$, indicating a constructive contribution of the destructive interference into the deficit of absorption.

In principle, in the case of stronger coupling, $\Omega \gg (\gamma_c - \gamma_a)/2$, the total absorption line could be viewed as the sum of two lines separated by 2Ω (similar to the case $\gamma_a = \gamma_c$) though with the deformed line shapes (as compared with the Lorentzian ones) due to interference effects.

In this case the line splitting should actually be noticeable (see Fig. 15). Moreover such strong coupling would apparently appear in the overall Mössbauer spectra and not just for merging lines (where it was observed experimentally).

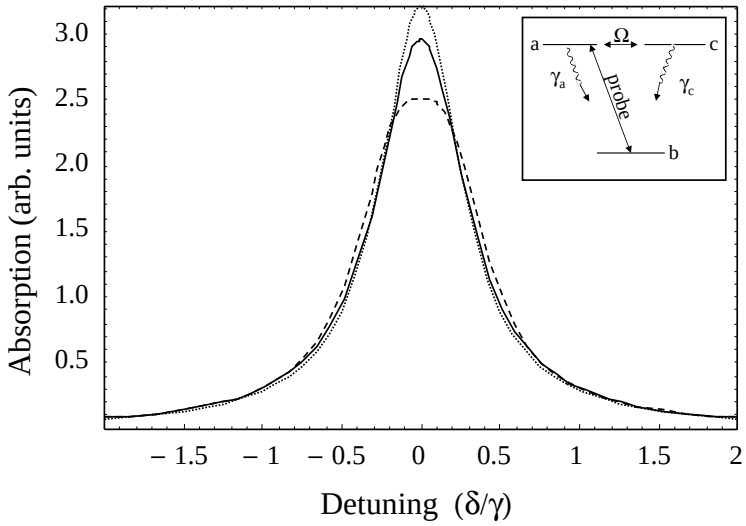

FIG. 16. Absorption curves for V_0^+ probing γ-radiation. (i) dotted line corresponds to $\Omega = 0$, $\gamma_c = 1$, and $\gamma_a = 0.31$; (ii) solid line corresponds to $\Omega = 0.1644\gamma_c$, $\gamma_c = 1$, and $\gamma_a = 0.31$; (iii) dashed line corresponds to $\Omega = 0.1644$, $\gamma_c = 0.31$, and $\gamma_a = 0.31$

Let us consider now the case when the linewidth at the transition probed by γ-radiation is narrower than at the adjacent transition. It corresponds to our experimental scheme with $\gamma_a < \gamma_c$ probed at $\Delta m = 1$, i.e. a-b, transition only. In this case the same formulas (see Eq. 3.10) can be used with a replacement of γ_c by γ_a and γ_a by γ_c. So that in the week coupling limit the positive Lorentzian is getting to be narrower than the negative one. Note that the deficit in absorption for a given γ_a caused by Ω is smaller for $\gamma_c > \gamma_a$ in this case than for $\gamma_a = \gamma_c$ indicating constructive contribution of the coherence between the dressed states to the absorption. The absorption curves for V_0^+ probing γ-radiation corresponding to the same cases as were considered before for V_0^- probe are given in Fig. 16. Note that an absorption deficit for V_0^+ probe at $\Omega = 0.1644$ is smaller than for V_0^- probe.

As it has already been noticed above, in the case of the unpolarized Mössbauer

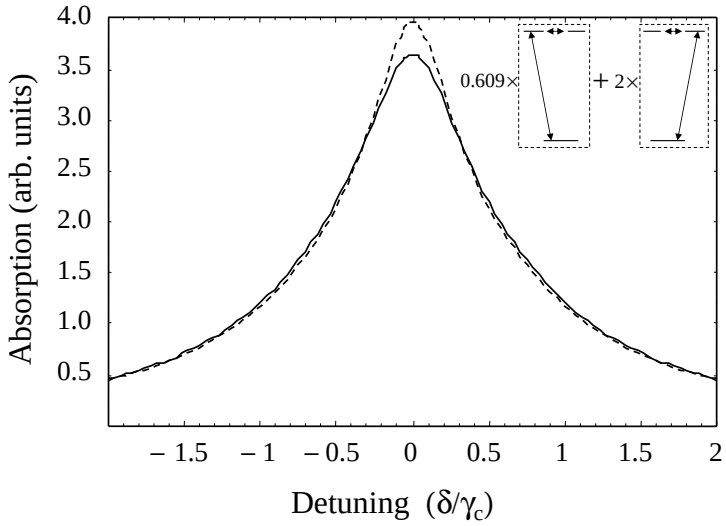

FIG. 17. Net absorption curves for unpolarized γ-radiation. (i) dashed line corresponds to $\Omega = 0$, $\gamma_c = 1$, and $\gamma_a = 0.31$; (ii) solid line corresponds to $\Omega = 0.1644\gamma_c$, $\gamma_c = 1$, and $\gamma_a = 0.31$.

source and single crystal absorber in the parallel geometry, the total absorption spectrum of a thin sample may be obtained just by summation of absorption for V_0^- and V_0^+ probes (see Fig. 17). The absorption deficit for $\Omega = 0.1644\gamma_c$ in this case is equal to 8%.

Thus we may conclude that nuclear interference effects should result in the absorption deficit under the level anti-crossing condition.

As it has been mentioned above, a breaking of an axial symmetry may occur either via electric quadrupole or magnetic interaction. However, a transverse component of a magnetic field does not provide a direct coupling between the crossing sublevels ($m = 1/2$ and $m = -3/2$). It couples them only in the second order via the sublevel $m = -1/2$ of the excited state manifold. Besides it leads to an additional coupling between the sublevels $m = 1/2$ and $m = 3/2$ in the excited state manifold and the sublevels $m = 1/2$ and $m = -1/2$ in the ground state manifold. As a result

of this, along with an absorption deficit at the crossing point, it would lead simultaneously to the appearance of additional lines in the Mössbauer spectra which were not observed experimentally.

Thus we focus on the case when mixing of the upper levels occurs via quadrupole interaction, which couples the crossing sublevels directly and does not lead to any additional couplings. In case of quadrupole coupling $\Omega = \sqrt{3}\eta V_q$, where $\eta = (V_{xx} - V_{yy})/V_{zz}$. Hence $\Omega = 0.1644\gamma_c$ corresponds to $\eta = 0.067$.

D. Conclusion

We experimentally observed a reduction of the resonant γ-ray absorption under the nuclear level crossing condition in the optically thin sample of $FeCO_3$. We analytically analyzed a simplified three-level model (including two crossing upper levels and the single lower state) assuming coupling between the crossing levels due to the axial symmetry breaking in the system and proved that the nuclear interference (similar to EIT at atomic transitions in optics) caused by this coupling may lead to suppression of the Mössbauer absorption at the level crossing point. Finally, we estimated that a week breaking of an axial symmetry via quadrupole interaction, $\eta = 0.067$, would result in the observed 8% deficit of the resonant absorption.

CHAPTER IV

CONCEPT OF SPINNING MAGNETIC FIELD AT MAGIC-ANGLE CONDITION FOR LINE NARROWING IN MÖSSBAUER SPECTROSCOPY*

A new technique for narrowing of Mössbauer resonances in crystals is suggested. Similar to high-resolution nuclear magnetic resonance spectroscopy, it uses a combined action of a continuous wave radio-frequency and dc magnetic field under a "magic-angle" condition. However, the condition itself is essentially different from the one known previously. Moreover, this technique suppresses the contribution of the dipole-dipole interaction to the energy of Mössbauer transition only (it does not suppress the contribution of the dipole-dipole interaction to the energy of individual levels). It works rather well even in the case of relatively strong dipole-dipole interaction.

A. Introduction

Since the experimental discovery of the Mössbauer effect (a physical phenomenon of resonant recoil-free emission and absorption of γ-ray photons by nuclei bound in a crystal) in 1957, it has been observed for nearly 100 nuclear transitions in about 80 nuclides distributed over almost half of all chemical elements. This effect forms the basis of Mössbauer spectroscopy (MS) which has a number of applications, especially in solid state physics and chemistry [70, 71, 72, 73, 74].

Fundamentally, the width of recoilless γ-ray resonances, Mössbauer resonances, is limited only by the radiative linewidth of the given nuclear transition. However, inhomogeneous broadening, $\delta\omega_{inh}$, often sets a limit on the width of Mössbauer res-

*Reprinted in full with permission from [69] as follows: Petr Anisimov, Yuri Rostovtsev, and O. Kocharovskaya, Physical Review B, **76**, 094422 (2007). http://link.aps.org/abstract/PRB/v76/e094422

onances. In particular for transitions with a lifetime longer than 10 μs, $\delta\omega_{inh}$ defines the ultimate width of Mössbauer resonances. Large inhomogeneous broadening of long-lived recoilless transitions, as compared to the radiative broadening, is the major factor restricting their applications in Mössbauer spectroscopy. (Homogeneous broadening caused by spin-lattice relaxation can be suppressed down to 0.1 Hz by cooling a sample below 1 K.) In the case of nuclear transitions with a lifetime shorter than 10 μs, $\delta\omega_{inh}$ may sometimes exceed the radiative linewidth and limit the resolution of MS. An example of such a transition is the 14.4 keV transition in ^{57}Fe. For this transition, the width of Mössbauer resonances in some compounds may be four to nine times larger than the radiative linewidth [75, 76]. Therefore, the suppression of inhomogeneous broadening would both improve the resolution of Mössbauer spectroscopy in the cases where an interaction with an environment prevents an accurate measurement and would allow for extension of the Mössbauer technique to the longer-lived isomers and for observing Mössbauer resonances narrower than those currently achieved.

Inhomogeneous broadening also sets a fundamental obstacle to the realization of a Mössbauer γ-ray laser. The original idea of the Mössbauer γ-ray laser was suggested in 1961 by Lev Rivlin [77]. For lasing to occur, the net gain should exceed off-resonant losses caused by ionization and Compton scattering of γ-radiation in crystals. The net resonant gain, in turn, is proportional to the ratio of the radiative linewidth over the total linewidth. For sufficiently long-lived isomers (for which pumping could be feasible) this ratio is very small. Thus, an increase of this ratio via the suppression of inhomogeneous broadening would lead to dramatic release in the amplification condition, as discussed in the literature devoted to the problem of γ-ray laser [78, 79].

The inhomogeneous broadening of Mössbauer resonances is caused by the inhomogeneities of hyperfine (HF)interactions. This mechanism is essentially the same

as in the case of nuclear magnetic transitions in solids. Very efficient methods of suppression of inhomogeneous broadening down to 0.1 Hz have been developed in high resolution solid state nuclear magnetic resonance spectroscopy (HRSSNMRS) [80]. The field of HRSSNMR started with the pioneering work of Raymond Andrew [81, 82]. He showed that mechanical spinning of a sample can greatly reduce the width of nuclear magnetic resonances if the axis of rotation makes a particular angle with a constant magnetic field. The same result was achieved by the application of a radio-frequency (RF) field without rotation of the sample [80]. Finally apart from the mechanical spinning of a sample, two different techniques have been developed. The first one uses sequences of resonant $\pi/2$ RF pulses [83, 84]. The second one exploits a slightly detuned continuous RF field satisfying a "magic-angle" condition [85]. Both techniques are based on the symmetry of the HF interactions which allows the suppression of the contribution of the HF interactions down to zero if such a contribution is sufficiently small.

For the last forty years, HRSSNMRS has been developed into the flourishing field of research and applications. Therefore, the extension of the techniques of HRSSNMRS to Mössbauer spectroscopy appears to be promising. The mechanical rotation of a sample would be inappropriate since MS essentially uses the Doppler effect for changing the transition frequency. However, the application of a rotating RF field is possible. The influence of the RF field on the Mössbauer resonance was widely studied theoretically since the 1960's [41]; see also [42, 43, 44, 45, 36] for reviews. Some coherent effects in MS caused by the RF field, such as collapse of the HF structure [53, 54, 55], ac-Stark splitting [46, 47, 48, 49], and two-photon gamma-RF transitions [50, 51, 52], were observed experimentally. The idea to apply the HRSSNMRS techniques to narrow Mössbauer resonances was pioneered in the 1970's. It was suggested to use sequences of $\pi/2$ RF pulses [86] or quasi-continuous RF fields [78]. The pecu-

liarity of MS as compared to HRSSNMRS lies in the presence of HF structure in an excited nuclear state as well as in a ground nuclear state. For example, the dipole-dipole interaction couples pairs of nuclei in a ground state as well as in an excited state; moreover, it couples pairs of nuclei one of which is in a ground and the other one is in an excited state. Thus, the idea presented in the previous papers [86, 78] was to suppress HF interactions both in ground and excited nuclear states. The outcome of such an approach would be simultaneous elimination of all possible contributions from HF interactions. The drawback of such an approach was the requirement for rather complicated sequence of cycles of bichromatic RF field. One RF frequency was meant to affect ground nuclear states while the other was supposed to affect excited nuclear states only. After all, line narrowing was still limited by the fact that each RF frequency was affecting both ground and excited nuclear states. As far as we know, no experimental attempts for the verification of this proposal were undertaken.

In our recent papers [87, 88], we considered the possibility to narrow Mössbauer resonances by a monochromatic cw RF field. We used a combination of a traditional "magic-angle" condition with effective time-averaging. It was shown that partial narrowing could be achieved and that an optimization of the parameters used is required for further improvement.

In this paper, we suggest an essentially different approach for the suppression of the inhomogeneous broadening of Mössbauer resonances caused by the dipole-dipole interaction. Namely, we look for a condition where the contribution of the dipole-dipole interaction to the frequency of a Mössbauer resonance vanishes under the action of a monochromatic continuous RF field. At the same time we are not attempting full suppression of the dipole-dipole interaction and its contributions to the energy of individual levels. The frequency of γ-ray absorption remains well-defined even though the energy of individual nuclear levels deviates significantly. This happens due to the

cancellation of these deviations when the energy difference is observed. In this way, we define the magic-angle condition for MS and show that efficient suppression of the inhomogeneous broadening of Mössbauer resonances becomes possible with one monochromatic continuous RF field.

B. Theoretical model

A typical Mössbauer experiment involves a nuclear transition between two levels, with energy separation of about 10-100 keV. Each nuclear level has sublevels with a definite projection of the nuclear moment onto a quantization axis. The energy separation of nuclear sublevels is on the order of 10 neV. These sublevels are actually responsible for the HF structure of observed spectra. In a typical Mössbauer setup, the flux of incident γ-photons from a radioactive source is not sufficient to excite several nuclei in the close vicinity of each other. Therefore, one can always consider that only one (primary) nucleus interacts with γ-radiation and the rest of the nuclei (of the same type as the primary nucleus or some different nuclei in the crystal host) represent the environment and can not be excited. For the sake of further discussion, we label the primary nucleus as "1" and a nucleus from the environment as "2"(see Fig. 18).

In order to introduce the inhomogeneous broadening in our system, we assume that the primary nucleus interacts with the environment through the dipole-dipole interaction. This is a short-range pairwise interaction, which depends on a distance r_0 between the nuclei in the pair and on a relative position $\mathbf{n}_0 = (\cos\phi\sin\theta, \sin\phi\sin\theta, \cos\theta)$ of the pair with respect to the axis of quantization (z-axis). Short-range interactions mostly involve the nearest nuclei. Therefore, we assume r_0 to be constant and equal to the distance between nuclei. Furthermore, due to the pairwise nature of the dipole-dipole interaction, we can reduce our system to the pair of nuclei, which contains the

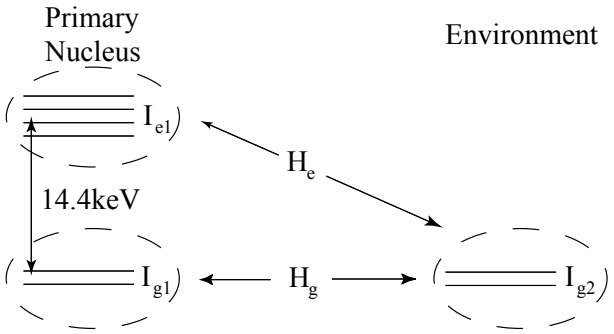

FIG. 18. Schematic representation of the studied system in the case of ^{57}Fe. H_g and H_e represent an interaction of the primary nucleus in the ground and excited states with its environment respectively.

primary nucleus and a nucleus from the environment. Thus in order to calculate a bulk response, one has to average the pairwise response over θ and ϕ.

Our system has a close resemblance to the one used to describe HRSSNMR except for the possibility of the primary nucleus to be in the excited state. Thus, there are two contributions to the width of Mössbauer resonances instead of one contribution to the width of nuclear magnetic resonances. The first contribution is due to the interaction of the primary nucleus in the ground state with the environment, H_g, and is also present in the case of HRSSNMR. The second contribution comes from the interaction of the primary nucleus in the excited state with the environment, H_e, and is specific for Mössbauer resonances. Thus, the HRSSNMR techniques have to be modified to consider this contribution.

For all further estimates and numerical simulations, we assume the primary nucleus to be ^{57}Fe in a soft ferromagnetic material [89]. Such nuclei experience a strong internal magnetization, which can be easily manipulated in soft ferromagnets by a rather weak external magnetic field. In principle, the environment may contain nuclei other than ^{57}Fe. However for further estimates, we also use all typical characteris-

tics of ^{57}Fe except for the magnitude of the dipole-dipole coupling constant. At the atomic distances, the dipole-dipole interaction between ^{57}Fe is relatively weak when compared to the width of the Mössbauer resonance. For the sake of demonstration, we assume that the dipole-dipole coupling constant $\eta \sim \mu_1\mu_2/r_0^3$ (where μ_i is the magnetic dipole moment of the i^{th} nucleus) is large enough to provide substantial inhomogeneous broadening of the Mössbauer spectrum.

In order to achieve the suppression of inhomogeneous broadening, we place the system in the external magnetic field which consists of two components: a constant component (this component defines the z-axis) and a time-dependent one. We choose the time-dependent component in such a way that the total external magnetic field spins around the z-axis: $\mathbf{B} = B_0\left(r\cos\omega_{rf}t, -r\sin\omega_{rf}t, 1\right)$. In the previous expression, we introduced r as the ratio of the magnitudes of the time-dependent and the constant components of the magnetic field.

The Hamiltonian of the system consisting of the pair of nuclei placed in the external magnetic field and coupled through the dipole-dipole interaction is written as follows ($\hbar = 1$):

$$H = -\mathbf{B}\left(\gamma_1\mathbf{I}_1 + \gamma_2\mathbf{I}_2\right) + \eta\left(\mathbf{I}_1\mathbf{I}_2 - 3\left(\mathbf{n}_0\mathbf{I}_1\right)\left(\mathbf{n}_0\mathbf{I}_2\right)\right), \tag{4.1}$$

where γ_i and $\mathbf{I}_i$ are the gyromagnetic ratio and the nuclear moment of the i^{th} nucleus. For our system, γ_1 and $\mathbf{I}_1$ are not fixed and depend on the state of the nucleus; however, γ_2 and $\mathbf{I}_2$ are fixed to $\gamma_g = 1.373$ MHz T^{-1} and $\mathbf{I}_g = 1/2$ respectively since the second nucleus can be in the ground state only. For the primary nucleus, the gyromagnetic ratio and the nuclear moment can also be equal to $\gamma_e = -0.787$ MHz T^{-1} and $\mathbf{I}_e = 3/2$ if the nucleus is in the excited state.

Depending on the state of the primary nucleus, the system can be in the ground

state described by the Hamiltonian

$$H_g = -\mathbf{B}\left(\gamma_g \mathbf{I}_{g1} + \gamma_g \mathbf{I}_{g2}\right) + \eta_g \left(\mathbf{I}_{g1}\mathbf{I}_{g2} - 3\left(\mathbf{n}_0\mathbf{I}_{g1}\right)\left(\mathbf{n}_0\mathbf{I}_{g2}\right)\right), \tag{4.2}$$

or in the excited state, with energy $\hbar\Omega_0 = 14.4$ keV, described by the Hamiltonian

$$H_e = -\mathbf{B}\left(\gamma_e \mathbf{I}_{e1} + \gamma_g \mathbf{I}_{g2}\right) + \eta_e \left(\mathbf{I}_{e1}\mathbf{I}_{g2} - 3\left(\mathbf{n}_0\mathbf{I}_{e1}\right)\left(\mathbf{n}_0\mathbf{I}_{g2}\right)\right), \tag{4.3}$$

where $\eta_e/\eta_g = \gamma_e/\gamma_g = -0.573$. The energy of the excited state is omitted here, a condition which is equivalent to the rotating wave approximation in quantum optics [90].

For H_g, we have two nuclei with $I_{g1} = 1/2$ and $I_{g2} = 1/2$, which leads to the basis $|1/2, m_1 = 1/2, -1/2\rangle \otimes |1/2, m_2 = 1/2, -1/2\rangle$. However, as shown in our previous work [88], the basis of the total moment, $|0,0\rangle$,$|1,1\rangle$, $|1,0\rangle$, and $|1,-1\rangle$, is the most useful for a system of two identical nuclei. This observation is based on the fact that a state with a total moment equal to zero $|0,0\rangle$ is not affected by magnetic interactions. Thus, it can be excluded from consideration.

For H_e, the primary nucleus has $I_{e1} = 3/2$, which leads to the basis $|3/2, m_1 = 3/2, ..., -3/2\rangle \otimes |1/2, m_2 = 1/2, -1/2\rangle$. In this case, there is no actual preference for the basis of the total moment.

The Mössbauer transition in the primary nucleus from the ground to the excited level is considered to be magnetic dipole-allowed (corresponding to the case of ^{57}Fe). It means that a transition operator can be written as $V = -\hat{\mu} \cdot \mathbf{B}_\gamma$. In the previous expression, we introduced the magnetic field of a γ-quantum, $\mathbf{B}_\gamma$, and the magnetic moment of the transition, $\hat{\mu}$. The magnetic moment $\hat{\mu}$ is proportional to $\sum_{m=-1}^{1} \hat{\mu}_m \cdot \mathbf{X}_m$, where $\left(\hat{\mu}_m\right)_{m_e,m_g} = \langle I_g, 1, -m_g, m| \, |I_e, m_e\rangle$ are the Clebsch-Gordan coefficients [91], and $\mathbf{X}_0 = \mathbf{z}_0$, $\mathbf{X}_{\pm 1} = \mp\left(\mathbf{x}_0 \pm i\mathbf{y}_0\right)/\sqrt{2}$. We assume that an incident γ-radiation propagates along the y-axis and can have either $\mathbf{B}_\gamma \parallel \mathbf{z}_0$ or $\mathbf{B}_\gamma \parallel \mathbf{x}_0$. Hence, the

transition operator is represented by the matrix V_z^0 in the case of $\mathbf{B}_\gamma \parallel \mathbf{z}_0$ or by the matrix V_x^0 in the case of $\mathbf{B}_\gamma \parallel \mathbf{x}_0$:

$$V_z^0 = K \begin{bmatrix} 0 & 0 \\ \sqrt{2} & 0 \\ 0 & \sqrt{2} \\ 0 & 0 \end{bmatrix}, V_x^0 = \frac{K}{\sqrt{2}} \begin{bmatrix} -\sqrt{3} & 0 \\ 0 & -1 \\ 1 & 0 \\ 0 & \sqrt{3} \end{bmatrix}, \tag{4.4}$$

where K is some constant which is irrelevant for further discussion. Here, the following basis for the primary nucleus is assumed: $|I_e = 3/2, m_e = 3/2, ..., -3/2\rangle$ for the excited and $|I_g = 1/2, m_g = 1/2, -1/2\rangle$ for the ground state. Finally, the transition matrices for our system of two nuclei with one nucleus confined to the ground state are $\tilde{V}_{x,z}^0 = V_{x,z}^0 \otimes \hat{1}_{2\times 2}$, which have to be transformed to the basis discussed above.

We calculate Mössbauer spectra based on the Floquet-state perturbation theory presented in [92, 87]. This theory was developed to study homogeneously broadened Mössbauer spectra under the influence of the RF field. It treats γ-radiation as a perturbation which is always the case for MS allowing for a nonperturbative treatment of the RF field. It is important to note that it also allows for a nonperturbative analysis of the dipole-dipole interaction. As far as we know, nobody has used this method to study inhomogeneously broadened Mössbauer spectra (the broadening caused by the dipole-dipole interaction). This theory predicts a time-averaged absorption spectrum to be the sum of the Lorentzians:

$$L = \left|V_k\left(e,g\right)\right|^2 \cdot \frac{2}{\pi} \frac{\Gamma}{\left(\Omega - \Omega_{n,m,k}\right)^2 + \Gamma^2}, \tag{4.5}$$

where $V_k\left(e,g\right) = T^{-1} \int_0^T \left\langle n_e\right| \tilde{V}_{x,z}^0 \left|m_g\right\rangle e^{ik\omega_{rf}t} dt$ is the k-th coefficient of the Fourier series of the matrix element of the transition operator $\tilde{V}_{x,z}^0$ between the Floquet states $|n_e\rangle$ and $|m_g\rangle$; $\Omega_{n,m,k} = \Omega_0 + E_{\{n\}}^e - E_{\{m\}}^g - k\omega_{rf}$ is the resonance frequency of the

corresponding transition.

C. Ground state magic-angle condition

The strength of the dipole-dipole interaction can be judged by $\eta_g/\left|\Delta_{eff}\right|$ - the ratio of the coupling constant to the Zeeman splitting in the effective magnetic field, which is defined in the Appendix A. If the ratio is small, then the dipole-dipole interaction can be treated by perturbation method. First, we consider the primary nucleus in the ground state and the ratio being small. In this case our system is described in the co-rotating frame of reference by a so-called truncated Hamiltonian (see Ref. [93]):

$$H_g^0 = -\gamma_g \left(\mathbf{B}_{eff}\right)_g \left(\mathbf{I}_{g1} + \mathbf{I}_{g2}\right) - \eta_g A \left(\mathbf{I}_{g1} \cdot \mathbf{I}_{g2} - 3 \left(\mathbf{I}_{g1}\right)_z \left(\mathbf{I}_{g2}\right)_z\right), \tag{4.6}$$

where I_{gi} is the nuclear moment of the i^{th} nucleus, γ_g - the gyromagnetic ratio and η_g - the dipole-dipole coupling for the ground state, and $A = 3\cos^2\theta - 1$ represents the dependence of the interaction Hamiltonian on the relative position of the nuclear pair. Eigenvalues of H_g^0 in the absence of the dipole-dipole interaction are $\{0, \Delta_{eff}, 0, -\Delta_{eff}\}$ (see Appendix A), which are the dynamical energy levels corresponding to the states dressed by the RF field with a corresponding total moment equal to zero for the first eigenvalue and one for the last three eigenvalues. The dipole-dipole interaction provides an additional contribution to the eigenvalues:

$$\left\{0, -\eta_g D\left(\theta_{eff}\right), 2\eta_g D\left(\theta_{eff}\right), -\eta_g D\left(\theta_{eff}\right)\right\}. \tag{4.7}$$

These linear corrections are proportional to $D\left(\theta_{eff}\right) = A\left(3\cos^2\theta_{eff} - 1\right)/8$, and thus can be set to zero all at once if

$$3\cos^2\theta_{eff} - 1 = 0. \tag{4.8}$$

This condition is well-known in solid state high resolution nuclear magnetic resonance spectroscopy as the magic-angle condition, which defines the magic-angle as: $\theta_{eff} = \arccos\left(1/\sqrt{3}\right)$.

D. Strong dipole-dipole interaction in the ground state

A typical value of the magnetic field experienced by ^{57}Fe in the soft ferromagnets is on the order of 30 T. In such a field, a Zeeman splitting is $|\Delta|/2\pi = 41.2$ MHz, i.e. it exceeds the radiative linewidth, which is equal to $2\Gamma/2\pi = 2.256$ MHz, only by a factor of 18. Thus if the inhomogeneous broadening caused by the dipole-dipole coupling exceeds the radiative linewith, then this coupling should be relatively strong, so that the ratio $\eta_g/|\Delta|$ can not be smaller than 1/18. In other words a range of the dipole-dipole coupling constants where the magic-angle condition works well is quite narrow: 2.256 MHz$< \eta_g/2\pi \ll 41.2$ MHz.

When the dipole-dipole constant becomes comparable or even exceeds Zeeman splitting $\eta_g/|\Delta_{eff}| \geq 1$, we cannot use perturbation theory anymore. In this case the energies of the ground state should be calculated numerically. We are going to use Floquet analysis according to the prescription outlined in the Appendix B.

Figure 19 presents quasi-energies (circles) of the Floquet states, which correspond to the states with a total nuclear moment equal to one, in the case $\eta_g/2\pi = 9.024$ MHz. There are more than three values at each particular frequency ω_{rf}, but unique points are confined to the first Floquet zone, which lies in between two dashed lines $\pm\omega_{rf}/2$.

In the absence of the dipole-dipole interaction, quasi-energies can be calculated analytically. They are represented by the solid lines marked as ε_1, ε_0, and ε_{-1}.

The frequencies of the RF field satisfying the magic-angle condition (defined by

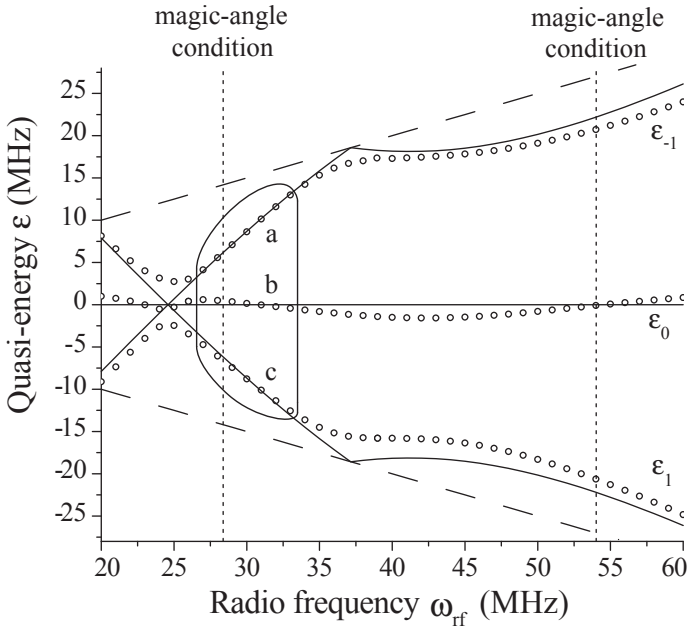

FIG. 19. Quasi-energies of H_g as a function of the RF frequency for the states with the total moment equal to one. These values, marked by circles, are calculated for the following set of parameters: $\eta_g/2\pi = 9.024$ MHz, $r = 0.44$, $\Delta/2\pi = 41.2$ MHz, $\theta = \pi/4$. Solid lines labeled by ε_1, ε_0 and ε_{-1} correspond to the quasi-energies of H_g calculated analytically in the absence of the dipole-dipole interaction. Dashed lines represent the limits of the Floquet zone. Vertical short-dashed lines correspond to the magic-angle condition. More detailed analysis of the selected region is presented in Fig. 20.

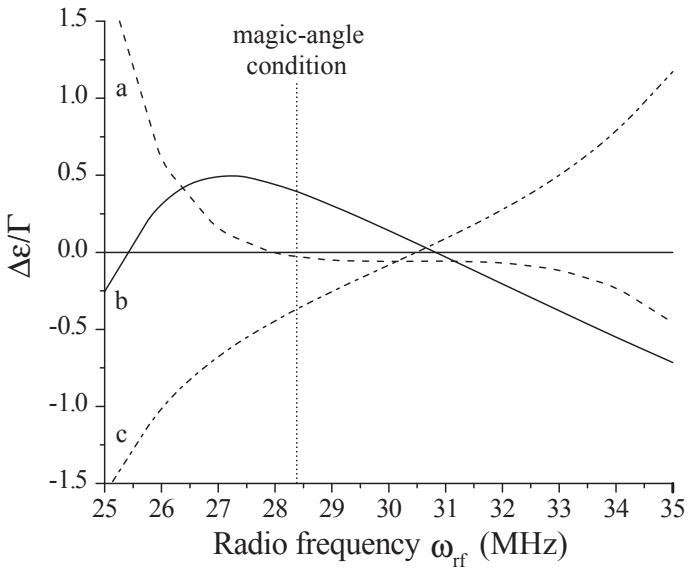

FIG. 20. The normalized difference between numerical value of the quasi-energy of the ground state and the value obtained analytically in the absence of the dipole-dipole interaction (see Eq. (4.9)) as a function of ω_{rf} is represented. The parameters are the same as in Fig. 19.

Eq. (4.8) for the chosen parameters) presented by the vertical short-dashed lines in Fig. 19.

As it is obvious from the Fig. 19, the higher value of the frequency satisfying to magic-angle condition (which lays above the nuclear magnetic resonance frequency for the ground state $\omega_{rf}/2\pi = 41.2$ MHz) does not correspond to the vanishing contribution of the dipole-dipole interaction to the ground state energy. It is less obvious for the lower value of the frequency. Therefore, we provide a closer look at the selected area in Fig. 20. Moreover, we plot the normalized difference between an exact numerical value of the energy and that obtained analytically in the absence of the dipole-dipole interaction:

$$\frac{\Delta\varepsilon}{\Gamma} = \frac{\varepsilon^{num} - \varepsilon^{0}}{\Gamma}. \tag{4.9}$$

As it follows from the Fig. 20, only ε_{-1} is unaffected by the dipole-dipole coupling at MAC. The contribution of the dipole-dipole interaction to ε_0 and ε_1 does not vanish at magic-angle condition. Finally, it is important to note that it is possible to minimize the ground state dipole-dipole contribution, if $\omega_{rf}/2\pi = 30.7$ MHz, for all three quasi-energies at once.

Let us study how the dipole-dipole coupling in the ground state affects a Mössbauer spectrum. For this purpose, we temporarily put $\eta_e = 0$ (see also [87]) and use the same coupling constant $\eta_g/2\pi = 9.024$ MHz as above. This coupling is strong enough to provide a noticeable broadening of the Mössbauer resonances (see Fig. 21). This figure contains contributions from x- and z-polarized γ-radiation which sums up to a total spectrum for unpolarized radiation. One can see that there are four major Mössbauer resonances: two for x- and two for z-polarized radiation which are marked accordingly as XR, XL, ZR, and ZL in Fig. 21.

We calculated Mössbauer absorption spectra for a broad range of parameters

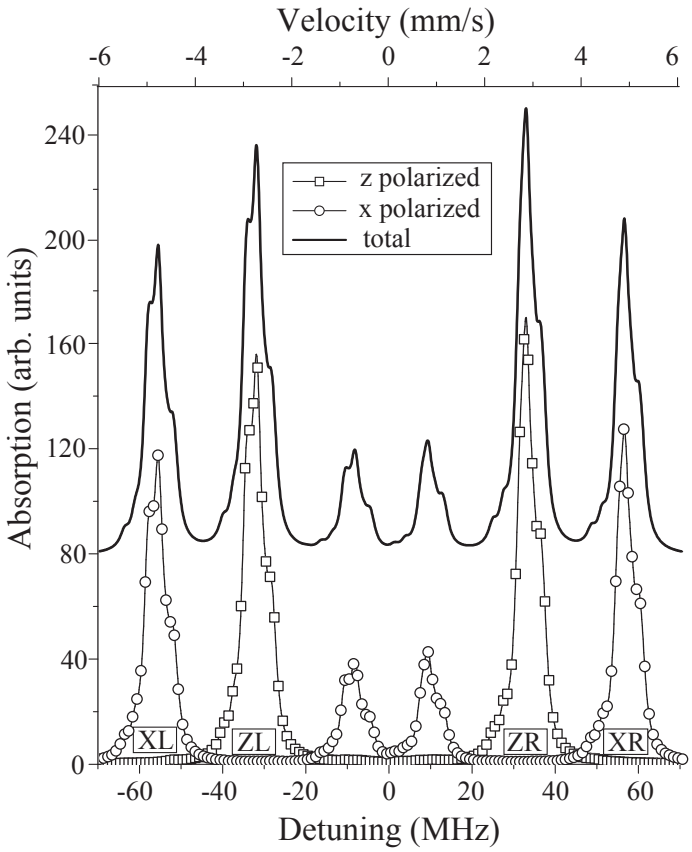

FIG. 21. Mössbauer absorption spectrum calculated in the presence of a constant magnetic field $B_0 = 30$ T and a strong dipole-dipole interaction in the ground state only: $\eta_g/2\pi = 9.024$ MHz and $\eta_e/2\pi = 0$ MHz. The dipole-dipole interaction results in a substantial broadening of the Zeeman sextet. The four strongest Mössbauer resonances are labeled accordingly: ZL and ZR for z-polarized radiation, and XL and XR for x-polarized radiation. A shift of 80 arb. units is introduced to separate the spectrum for unpolarized radiation from its polarized contributions.

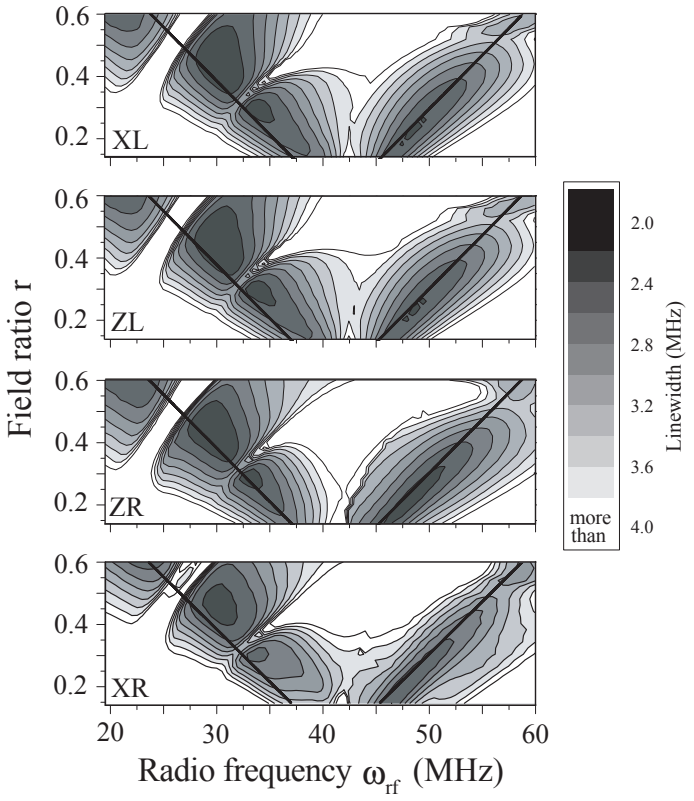

FIG. 22. The dependence of the width of the four major Mössbauer resonances on the frequency ω_{rf} and the relative strength r of the RF field is presented. All parameters are the same as in Fig. 21. A shade coding is used, such that the darker shade corresponds to the smaller width of a resonance. In order to provide a better resolution, values greater than 4 MHz are whited out. Along solid lines ω_{rf} and r satisfy to the ground state magic angle condition defined by Eq. (4.8).

of the RF field. Figure 22 presents dependence of the width of the four strongest Mössbauer resonances on the relative strength r (vertical scale) and the frequency ω_{rf} (horizontal scale) of the RF magnetic field. As it could be expected, the regions, where the linewidth reaches its minimal value, extend along the solid lines defined by the magic angle condition (see Eq. (4.8)). However, due to the large strength of the dipole-dipole interaction, the actual minima for XR and ZR, which involve ε_1, are shifted to the higher values of ω_{rf}. This result could be expected based on the behavior of ε_1 described in the beginning of this section.

Table I summarizes the analysis of the ground state contribution to the width of Mössbauer resonances and contains numerical values of the ground state contribution to the width of the four major Mössbauer resonances. This contribution was estimated as $\Delta\omega_d = \Delta\omega_{inh} - 2\Gamma$, where $\Delta\omega_{inh}$ is the total linewidth and 2Γ is the linewidth in the absence of the dipole-dipole interaction. The first row of Table I presents the dipole-dipole contributions in the absence of the RF field. The next four rows show absolute minima of $\Delta\omega_d$ for each of the four strongest Mössbauer resonances with corresponding labels presented in the last column. The last row of Table I corresponds to the minimum of the function defined as follows

$$F\left(r, \omega_{rf}\right) = 0.5 \sum_{\alpha\&\beta\in\Omega} \left(\left(\Delta\omega_d\right)_\alpha - \left(\Delta\omega_d\right)_\beta\right)^2, \tag{4.10}$$

where $\Omega = \{XL, ZL, ZR, XR\}$, and $\left(\Delta\omega_d\right)_\alpha$ is a contribution of the dipole-dipole coupling to the width of the Mössbauer resonance marked by α.

A final conclusion of this section is that suppression of the ground state contribution is possible. However, it does not happen at the magic angle condition and needs an adjustment of the parameters. Moreover, efficient suppression requires different sets of parameters for each Mössbauer resonance. Nevertheless, Table I shows that a

TABLE I. Contribution of the ground state dipole-dipole coupling to the width of the four strongest Mössbauer resonances. The first row presents contributions in the absence of the RF field. The next four rows present residual contributions after applying the RF field. Each row corresponds to maximal suppression for a particular Mössbauer resonance, specified in the last column. The last row presents parameters and values corresponding to the case when function defined in Eq. (4.10) reaches minimum, which means that all four Mössbauer resonances have residual contributions of the same order.

ω_{rf}, MHz	r	$\Delta\omega_d$ for XL, MHz	$\Delta\omega_d$ for ZL, MHz	$\Delta\omega_d$ for ZR, MHz	$\Delta\omega_d$ for XR, MHz	Abs min for
0	0	3.2546	3.3171	3.7089	3.6831	-
29.66	0.4614	0.1716	0.1814	0.2054	0.1953	XL
30	0.4517	0.1781	0.1651	0.2012	0.2068	ZL
29.56	0.4398	0.1848	0.1809	0.1857	0.1891	ZR
29.39	0.4472	0.1846	0.1911	0.1921	0.1861	XR
29.989	**0.4108**	**0.19845**	**0.19863**	**0.20071**	**0.20102**	**Optimal**

compromise can be found and an equivalent suppression can be achieved simultaneously for all the strongest Mössbauer resonances (see Fig. 23).

E. Excited state "magic-angle" condition

In this section, we consider the primary nucleus in the excited state. When the contribution of the dipole-dipole interaction to the energy of the excited state is small, $\eta_e / |\Delta_{eff}| \ll 1$ it can be treated perturbatively, similar to the analysis carried out for the ground state in Section D. In a co-rotating frame of reference, the truncated Hamiltonian for the excited state (taking into account the dipole-dipole coupling in the first order of the perturbation theory) takes a form:

$$H_e^0 = -\gamma_e \left(\mathbf{B}_{eff}\right)_e \cdot \mathbf{I}_{e1} - \gamma_g \left(\mathbf{B}_{eff}\right)_g \cdot \mathbf{I}_{g2} + \eta_e A \left(\mathbf{I}_{e1} \cdot \mathbf{I}_{g2} - 3 \left(\mathbf{I}_{e1}\right)_z \left(\mathbf{I}_{g2}\right)_z\right), \quad (4.11)$$

where $\left(\mathbf{B}_{eff}\right)_g$ and $\left(\mathbf{B}_{eff}\right)_e$ are the different effective magnetic fields for the magnetic dipole moments in the ground and excited state respectively; $I_{(g/e)i}$ and $\gamma_{g/e}$ are the nuclear moment of the i^{th} nucleus and the gyromagnetic ratio for the ground/excited state; η_e - the dipole-dipole coupling for the excited state, and $A = 3\cos^2\theta - 1$ represents a dependence on the relative position. Eigenvalues of H_e^0 in the absence of the dipole-dipole interactions are

$$\frac{3}{2}\Delta_{eff}^e \pm \frac{1}{2}\Delta_{eff}^g, \quad (4.12)$$

$$\frac{1}{2}\Delta_{eff}^e \pm \frac{1}{2}\Delta_{eff}^g, \quad (4.13)$$

$$-\frac{1}{2}\Delta_{eff}^e \pm \frac{1}{2}\Delta_{eff}^g, \quad (4.14)$$

$$-\frac{3}{2}\Delta_{eff}^e \pm \frac{1}{2}\Delta_{eff}^g, \quad (4.15)$$

(see Appendix A).

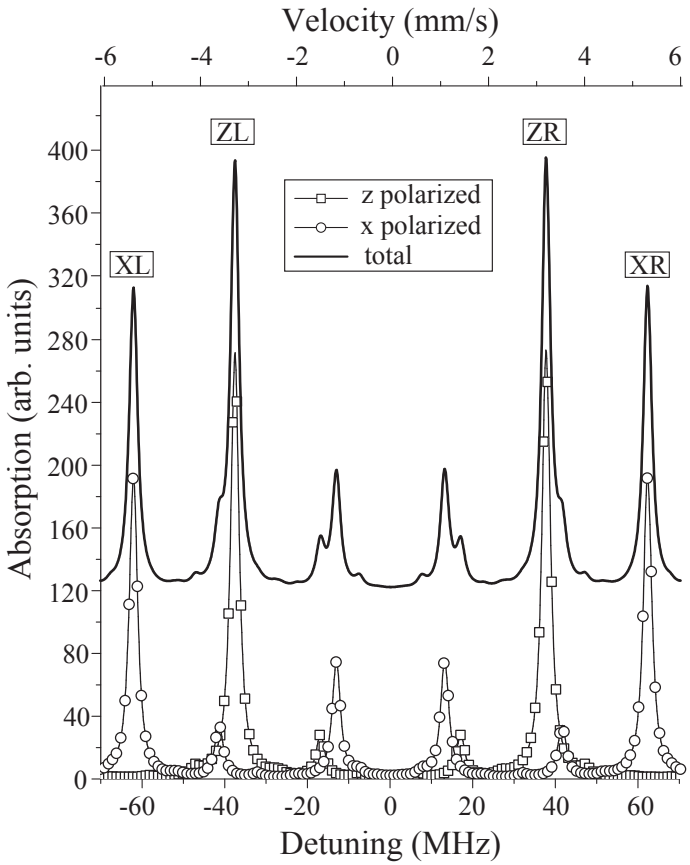

FIG. 23. Mössbauer absorption spectrum calculated in the presence of the spinning magnetic field with the following parameters: $B_0 = 30$ T, $r = 0.4108$, $\omega_{rf}/2\pi = 29.989$ MHz. The dipole-dipole coupling constants are $\eta_g/2\pi = 9.024$ MHz and $\eta_e/2\pi = 0$ MHz. A shift of 120 arb. units is introduced to separate the spectrum for unpolarized radiation from its polarized contributions. The residual ground state contribution to the width of the strongest Mössbauer resonances is given in Table I.

Since there are two different effective fields, the magic angle condition for only one effective angle becomes meaningless now. Nevertheless, some condition connecting two parameters of the RF field, namely, its relative strength r and its frequency ω_{rf}, can be derived based on the requirement of vanishing of the linear order corrections to the energy of the excited state.

$$\left\{\mp 3\eta_e\tilde{D}, \mp\eta_e\tilde{D}, \pm\eta_e\tilde{D}, \pm 3\eta_e\tilde{D}\right\}. \tag{4.16}$$

These corrections are proportional to the following function of the two arguments

$$\tilde{D}\left(\theta^g_{eff}, \theta^e_{eff}\right) = \frac{A}{8}\left(3\cos^2\left(\frac{\theta^e_{eff}+\theta^g_{eff}}{2}\right) - 1 - \sin^2\left(\frac{\theta^e_{eff}-\theta^g_{eff}}{2}\right)\right), \tag{4.17}$$

which reduces to $D\left(\theta_{eff}\right)$ in the case of $\theta^e_{eff} = \theta^g_{eff}$. Zero values of $\tilde{D}\left(\theta^g_{eff}, \theta^e_{eff}\right)$ define the following condition for the suppression of the linear order correction to the energy of the excited state:

$$3\cos^2\left(\frac{\theta^e_{eff}+\theta^g_{eff}}{2}\right) - 1 - \sin^2\left(\frac{\theta^e_{eff}-\theta^g_{eff}}{2}\right) = 0. \tag{4.18}$$

F. Strong dipole-dipole interaction in the excited state

When the dipole-dipole coupling constant η_e becomes comparable or even exceeds Zeeman splitting in the excited state, the dipole-dipole interaction cannot be treated perturbatively. Similar to the case of the ground state, the energies of the excited state can be calculated numerically using Floquet analysis.

Modification of the Mössbauer absorption spectrum due to the dipole-dipole interaction in the excited state is demonstrated in Fig. 24. Here we assume that $\eta_e/2\pi = -5.171$ MHz and $\eta_g = 0$. According to the relationship $\eta_e = (\gamma_e/\gamma_g)\eta_g = -0.573\eta_g$, the dipole-dipole coupling constant $\eta_e/2\pi = -5.171$ MHz corresponds to the previously used ground state coupling constant $\eta_g/2\pi = 9.024$ MHz.

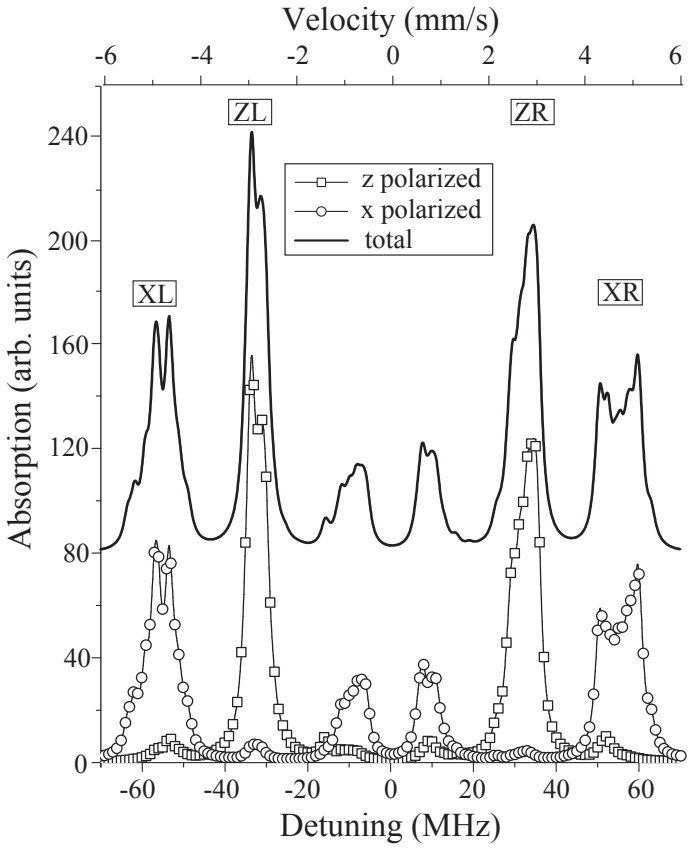

FIG. 24. Broadening of the Mössbauer resonances caused by the dipole-dipole interaction in the excited state assuming that $\eta_e/2\pi = -5.171$ MHz and $\eta_g = 0$. The shift of 80 arb. units is introduced to separate the spectrum for unpolarized radiation from its polarized contributions.

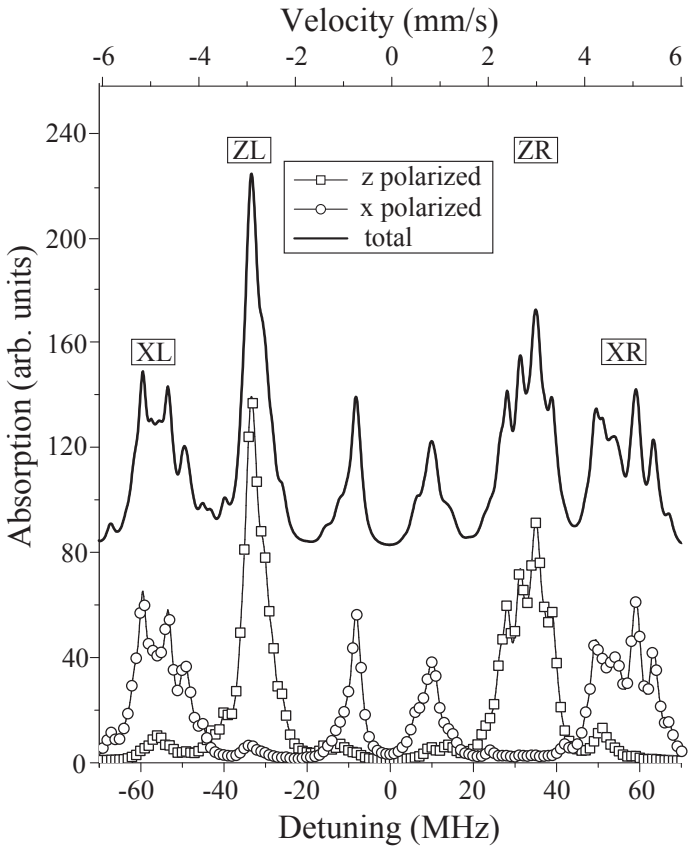

FIG. 25. Mössbauer absorption spectrum broadened due to the dipole-dipole interaction in both ground and excited states in the absence of the RF field. $B_0 = 30$ T, $\eta_g/2\pi = 9.024$ MHz, $\eta_e/2\pi = -0.573\eta_g/2\pi = -5.171$ MHz. A shift of 80 arb. units is introduced to separate the spectrum for unpolarized radiation from its polarized contributions.

TABLE II. Comparison of the contributions due to the dipole-dipole couplings in the ground, excited or both ground and excited states to the width of the Mössbauer resonances in the absence of the RF field.

$\Delta\omega_d$ for XL, MHz	$\Delta\omega_d$ for ZL, MHz	$\Delta\omega_d$ for ZR, MHz	$\Delta\omega_d$ for XR, MHz	$\eta_g/2\pi$, MHz	$\eta_e/2\pi$, MHz
3.2546	3.3171	3.7089	3.6831	9.024	0
5.9498	3.4867	5.5633	9.3575	0	-5.171
10.9444	7.8394	7.9814	13.8331	9.024	-5.171

The contribution of the dipole-dipole couplings in the ground and excited states to the widths of the Mössbauer resonances can be seen in the Table II. Note that the contribution to the excited state, $\Delta\omega_d$, for x-polarized radiation is larger than for z-polarized radiation. It is due to the fact that the corresponding transitions involve states with three times larger projection of the nuclear moment. Finally, when both contributions are combined, the Zeeman sextet becomes hard to recognize (see Fig. 25) because inhomogeneous broadening becomes comparable to the separation between the Mössbauer resonances (see the last row of Table II).

G. Magic angle condition for narrowing of the Mössbauer resonances

In order to suppress the dipole-dipole coupling both in the ground and excited states (when this coupling is relatively week) in the presence of the spinning magnetic field, two different magic angle conditions derived above (Eq. (4.8) and Eq. (4.18)) should be fulfilled. However, it is easy to see that it is impossible to satisfy both conditions simultaneously. On the other hand, these are not the energies of the excited and ground state themselves but their difference, $E^e_{\{n\}}-E^g_{\{m\}}$, which defines the frequencies of the Mössbauer resonances. Therefore, there is no need to suppress the contribution of the dipole-dipole interaction to the energies of the excited and ground states, rather, we have to make these contributions equal to each other in order for the frequencies of the Mössbauer transitions to remain unaffected by the dipole-dipole coupling. The following equation expresses this requirement mathematically:

$$\eta_g \left(3\cos^2\theta^g_{eff}-1\right) = \kappa\eta_e \left(3\cos^2\left(\frac{\theta^e_{eff}+\theta^g_{eff}}{2}\right)-1-\sin^2\left(\frac{\theta^e_{eff}-\theta^g_{eff}}{2}\right)\right), \quad (4.19)$$

where $\kappa = \pm 0.5$, ± 1, ± 1.5, and ± 3. The choice of κ depends on the Floquet states, which contribute to the particular Mössbauer resonance. This condition provides the

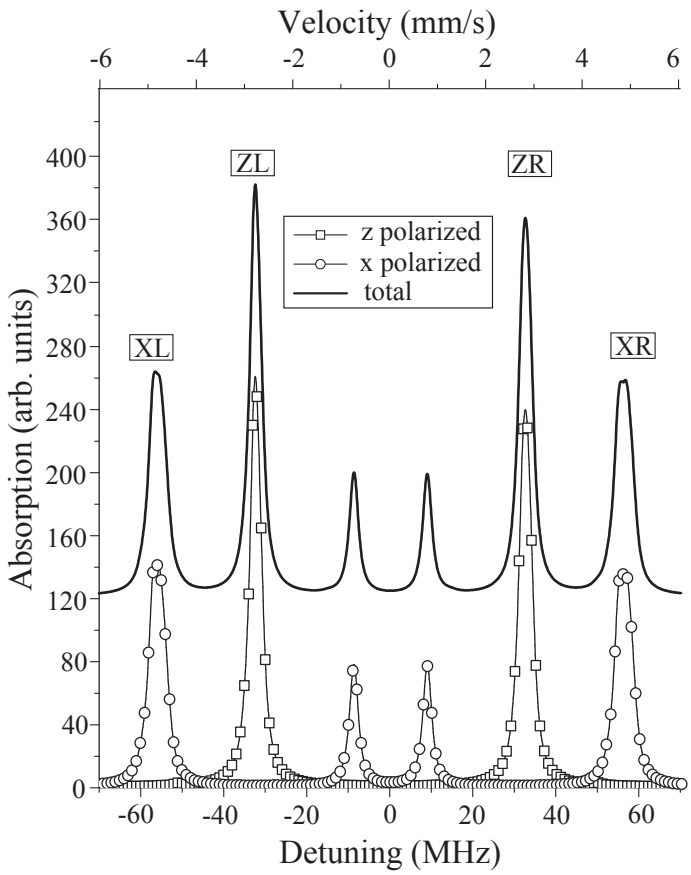

FIG. 26. Mössbauer absorption spectrum calculated in the absence of the RF magnetic field. $B_0 = 30$ T, $\eta_g/2\pi = 2.256$ MHz and a corresponding $\eta_e/2\pi = -1.2927$ MHz. A shift of 120 arb. units is introduced to separate the spectrum for unpolarized radiation from its polarized contributions.

suppression of the dipole-dipole contribution to a particular Mössbauer resonance by applying only one spinning magnetic field.

We demonstrate it numerically choosing $B_0 = 30$ T, $\eta_g/2\pi = 2.256$ MHz and $\eta_e/2\pi = (\gamma_e/\gamma_g)\eta_g = -0.573\eta_g = -1.2927$MHz.

The initial Mössbauer absorption spectrum (in the absence of the RF field) is shown in Fig. 26. This spectrum has a well-defined Zeeman sextet and a noticeable contribution from the dipole-dipole interaction to the width of Mössbauer resonances. Numerical values of this contribution to the four strongest Mössbauer resonances are given in the first row of Table III.

We calculated the Mössbauer absorption spectra for a broad range of the parameters of the RF field. Figure 27 presents the width of the four strongest Mössbauer resonances as a function of the relative strength r (vertical scale) and the frequency ω_{rf} (horizontal scale) of the RF magnetic field. It clearly follows from Fig. 27 that the regions, where maximal suppression of the inhomogeneous broadening is obtained, are aligned along thick lines corresponding to the magic angle condition determined by Eq. (4.19). Mössbauer resonances with x-polarized radiation are described by the condition with $\kappa = \pm 1.5$ (dashed) and $\kappa = \pm 3$ (solid) while Mössbauer resonances with z-polarized radiation are described by the condition with $\kappa = \pm 0.5$ (dashed) and $\kappa = \pm 1$ (solid). When ω_{rf} passes through the resonance for the ground state, κ changes sign since the effective magnetic field for the ground state changes the direction. Positive κ corresponds to the frequencies below the ground state resonance, and negative κ corresponds to the frequencies above the resonance.

Table III contains the sets of the parameters for which the best line narrowing in the case of individual Mössbauer resonance is achieved. The last row in Table III corresponds to the somewhat balanced case defined by the minimum of the function defined in Eq. (4.10), when broadening of the four strongest Mössbauer resonances

reaches common minimal broadening. The Mössbauer spectrum corresponding to this optimal set of the parameters, $r = 0.4796$ and $\omega_{rf}/2\pi = 31.90$ MHz, is presented in Fig. 28. In addition, Figure 29 compares this optimal configuration with the initial Mössbauer spectrum, presented in Fig. 26. One can easily see that the line narrowing effect takes place.

H. Conclusion

In this work, we suggested a new technique for suppression of inhomogeneous broadening of Mössbauer resonances. This technique relies on the mutual compensation of the contributions of HF interactions to the ground and excited states rather than total suppression of HF interactions. It is based on the combined action of the continuous wave RF and dc-magnetic fields satisfying the specific "magic-angle" condition Eq. (4.19). This technique is demonstrated numerically in a simple model dealing with a specific HF interaction, namely the dipole-dipole interaction. It can be generalized for other types of HF interactions, in particular the quadrupole interaction, exhibiting similar symmetry with respect to rotation.

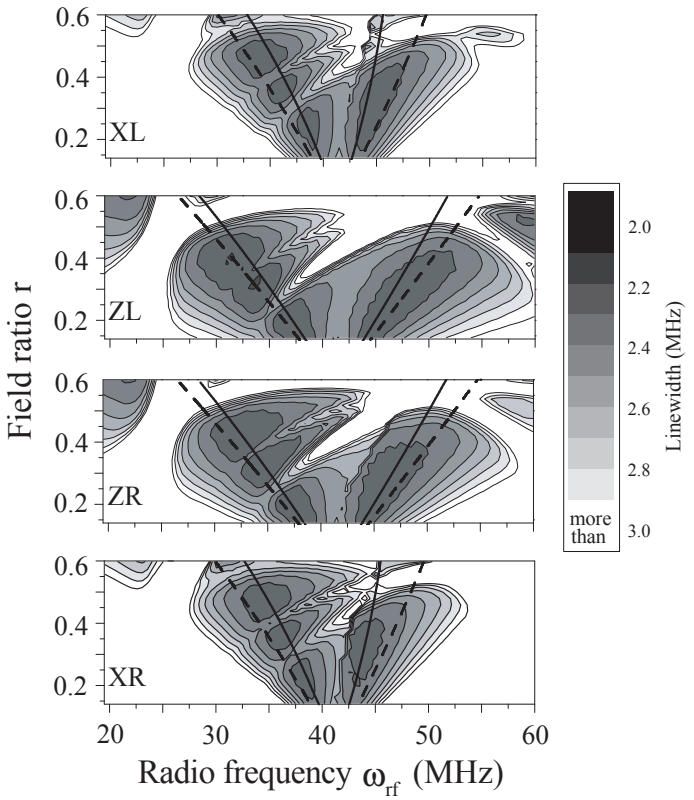

FIG. 27. Dependence of the width of the four strongest Mössbauer resonances on ω_{rf} and r is presented for $B_0 = 30$ T, $\eta_g/2\pi = 2.256$MHz, $\eta_e/2\pi = -1.2927$ MHz. The shade coding is used such that the darker shade corresponds to the narrower resonance. To provide better resolution, values greater than 3 MHz are not shown. The regions, where maximal suppression of the inhomogeneous broadening is obtained, are aligned along thick lines corresponding to the magic angle condition determined by Eq. (4.19).

TABLE III. Broadening of the four strongest Mössbauer resonances caused by the dipole-dipole interaction for $\eta_g/2\pi = 2.256$ MHz and a corresponding $\eta_e/2\pi = -1.2927$ MHz. The last row presents parameters and values corresponding to the case when function defined in Eq. (4.10) reaches minimum, which means that all four Mössbauer resonances have residual contributions of the same order.

ω_{rf}, MHz	r	$\Delta\omega_d$ for XL, MHz	$\Delta\omega_d$ for ZL, MHz	$\Delta\omega_d$ for ZR, MHz	$\Delta\omega_d$ for XR, MHz	Abs min for
0	0	2.648	1.017	1.436	2.894	-
33.55	0.4701	0.0809	0.1489	0.0996	0.0920	XL
31.50	0.4000	0.2727	0.0326	0.0722	0.2973	ZL
32.00	0.4310	0.1689	0.0516	0.0591	0.1946	ZR
35.30	0.4504	0.0858	0.1747	0.0934	0.0842	XR
31.90	**0.4796**	**0.1332**	**0.1568**	**0.1270**	**0.1511**	**Optimal**

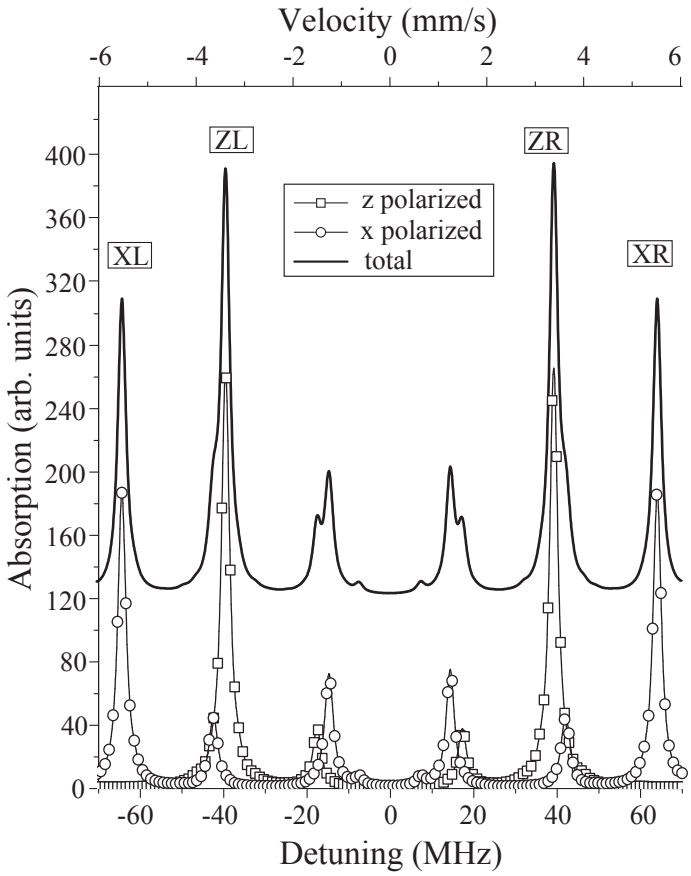

FIG. 28. Mössbauer absorption spectrum calculated in the presence of the spinning magnetic field. It illustrates the Mössbauer lines narrowing at the optimal set of the parameters, $r = 0.4796$ and $\omega_{rf}/2\pi = 31.90$ MHz. A shift of 120 arb. units is introduced to separate the spectrum for unpolarized radiation from its polarized contributions. The residual broadening of the Mössbauer resonances can be found in Table III.

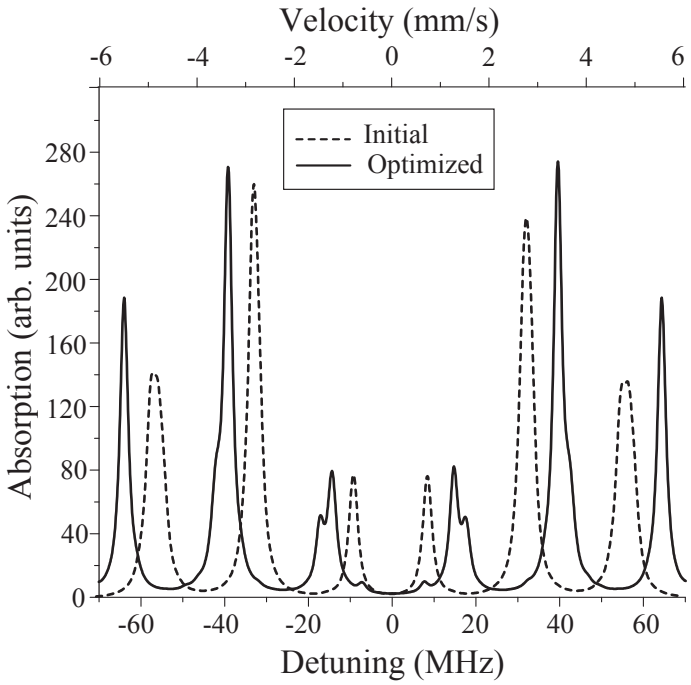

FIG. 29. The comparison of the initial Mössbauer spectrum presented in Fig. 26 with the narrowed spectrum presented in Fig. 28.

CHAPTER V

SUPPRESSION OF NUCLEAR ELASTIC FORWARD SCATTERING IN EXPERIMENTS WITH TRAINS OF ULTRASHORT PULSES*

We study nuclear elastic forward scattering of synchrotron radiation. In a simple model, we show that suppression of nuclear excitation by synchrotron radiation as well as nuclear elastic forward scattering are possible due to the formation of nuclear coherent population trapping. We consider a nucleus with ground- and excited-state nuclear momenta $I_g = 3/2$, $I_e = 1/2$, respectively. We demonstrate that nuclear coherent population trapping can be achieved for random phases of pulses in synchrotron radiation.

A. Introduction

The coherence excited by laser radiation in atoms is responsible for a variety of interference phenomena. These phenomena include coherent population trapping (CPT) [22, 20], electromagnetically induced transparency (EIT) [95, 24], lasing without population inversion (LWI) [96], slow light [27], and many others. The interest in these phenomena is fueled by many applications such as storage and processing of quantum information, ultrasensitive magnetometry, metrology, the development of lasers in vacuum ultraviolet (VUV), X-ray and γ-ray ranges, enhanced nonlinear optical conversions, etc. Nevertheless, CPT and related phenomena have not been demonstrated in the X-ray and γ-ray ranges, except for EIT in Mössbauer absorption [60].

It was predicted in Ref. [22] and shown in recent experiments [97, 30] that a

*This is a pre-print version of "Suppression of nuclear elastic forward scattering in experiments with trains of ultrashort pulses" by Petr Anisimov, Yuri Rostovtsev and Jos Odeurs from Journal of Modern Optics (2006) vol. 53 (16 & 17), pp. 2459 - 2467 [94]. Reprinted with permission by Taylor & Francis. http://www.informaworld.com

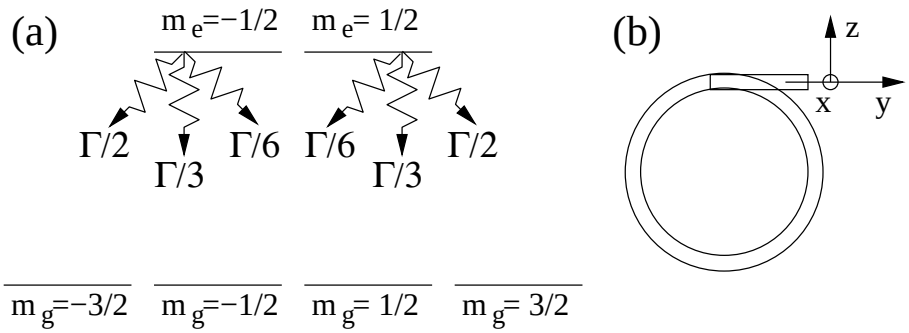

FIG. 30. (a) Level structure and decay channels of the nucleus with ground- and excited-state nuclear angular momenta $I_g = 3/2$, $I_e = 1/2$, respectively. (b) The choice of coordinate system with respect to the synchrotron source.

train of short optical pulses interacting with a three-level atom can effectively excite a coherence between ground states if the ground-state splitting is a multiple of the pulse repetition frequency $1/T$. We believe that it is possible to use synchrotron radiation as a source of a periodic train of short pulses to create CPT in nuclei. This would be the first demonstration of CPT in the X-ray range that can be used to suppress nuclear elastic forward scattering of synchrotron radiation and provide the conditions for studying electronic scattering alone.

In the next section, we describe the model studied in this paper. The results obtained are presented in Sec. C, and a conclusion is drawn in Sec. D.

B. System description

To illustrate the excitation of nuclear CPT by the synchrotron radiation, consider a nucleus with ground- and excited-state nuclear angular momenta $I_g = 3/2$, $I_e = 1/2$, respectively. The level structure of such a nucleus and the decays for magnetic dipole-allowed transitions are presented in Fig. 30(a). Figure 30(b) shows the frame of

reference used in this paper with respect to the synchrotron radiation. Consider further a magnetic field in the simplest configuration, $\mathbf{B} \parallel \hat{\mathbf{z}}_0$, which results in the Zeeman interaction described by ($\hbar$=1)

$$H_{(e,g)} = -\gamma_{(e,g)} \left(I_{(e,g)}\right)_z B_z, \tag{5.1}$$

where $\gamma_{(e,g)}$ and $\left(I_{(e,g)}\right)_z$ are gyromagnetic ratios and z-projections of the excited- and ground-state nuclear angular momenta of the nucleus, respectively. Numerical values of the gyromognetic ratio are based on the values of ^{57}Fe: $\gamma_g = 1.373$ MHz T^{-1} and $\gamma_e = -0.787$ MHz T^{-1}.

The Mössbauer transitions from the ground to the excited states are magnetic dipole-allowed, which means that the transition probability amplitude is proportional to $V = -\hat{\mu} \cdot \mathbf{B}_\gamma$. In the transition operator V, we introduced $\mathbf{B}_\gamma$, the magnetic field of the gamma quantum, in order to describe the polarization of the gamma quantum, and the magnetic moment of the transition $\hat{\mu}$ to characterize the coupling. The magnetic moment is proportional to $\sum_{m=-1}^{1} \hat{\mu}_m \mathbf{X}_m$, where $\left(\hat{\mu}_m\right)_{m_e,m_g} = \langle I_g, 1, -m_g, m |\, I_e, m_e \rangle$ is the Clebsch-Gordan coefficient [91], and $\mathbf{X}_0 = \mathbf{z}_0$, $\mathbf{X}_{\pm 1} = \mp(1/\sqrt{2})\left(\mathbf{x}_0 \pm i\mathbf{y}_0\right)$. In the frame of reference defined in Fig. 30(b), the incoming γ-radiation propagates along the direction of the y axis; therefore, $\mathbf{B}_\gamma$ is parallel to $\mathbf{x}_0$, which results in two independent Λ-systems (see Fig. 31), and the transition matrix in the basis $|I_g = 3/2, m_g = 3/2, ..., -3/2\rangle$ for the ground state and $|I_e = 1/2, m_e = 1/2, -1/2\rangle$ for the excited state is given by

$$V_x^+ = -\Omega\left(t\right) \begin{bmatrix} \frac{1}{\sqrt{2}} & 0 \\ 0 & \frac{1}{\sqrt{6}} \\ -\frac{1}{\sqrt{6}} & 0 \\ 0 & -\frac{1}{\sqrt{2}} \end{bmatrix}, \tag{5.2}$$

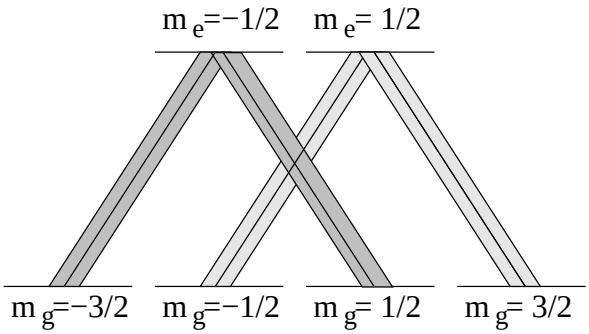

FIG. 31. Two independent Λ-systems are created by radiation with $\mathbf{B}_\gamma \parallel \mathbf{x}_0$. Transitions caused by such a radiation are shown as solid lines. Individual Λ-systems are highlighted by different shadings.

where $\Omega(t) = \sum_{n=0}^{\infty} \Omega_{max} \exp(-(t - nT)^2/2\tau^2)$ with the values of the parameters Ω_{max}, T and τ are based on the parameters of the transition and the properties of the incoming X-ray radiation. The period of this function, T, is defined by the repetition rate of the synchrotron source and is equal to 153 ns in the case of the Advanced Photon Source at Argonne. The duration of each pulse, $2\tau = 200$ ps, is about the duration of pulses for the X-ray source mentioned above. The last parameter Ω_{max} depends on the intensity of the X-ray source and the dipole moment of the transition. The choice of the intensity of the X-ray radiation is not addressed in this paper; thus, the numerical value of $\Omega(t)$ is chosen to create the coherence within the reasonable time interval. Furthermore, we take Ω_{max} with a phase, which can be random. The ability to use pulses with random phases is important because there is no phase control of the synchrotron radiation. Our final assumption is a finite lifetime of the ground state coherence; however, such a coherence can live very long and lifetimes of 100 μs to 1 ms seems reasonable [93].

The total Hamiltonian of the system in the rotating wave approximation is

$$H = \begin{bmatrix} H_g & V_x^+ \\ V_x & H_e \end{bmatrix}. \tag{5.3}$$

For further discussion, we assign labels 1 to 4 to the states $|I_g = 3/2, m_g = 3/2, ..., -3/2\rangle$ and 5 to 6 to the states $|I_e = 1/2, m_e = 1/2, -1/2\rangle$.

C. Obtained results

We carried out a numerical simulation of the system. For the simulation, we used the fourth/fifth order Runge-Kutta method to solve the set of ordinary differential equations

$$\frac{d\rho}{dt} = -i\,[H, \rho] - \hat{\Gamma}\rho. \tag{5.4}$$

where ρ is the density matrix of the system; $\hat{\Gamma}\rho$ is a symbolic notation for the proper decay rates of the populations and coherences in the system. The result of the numerical simulation is the density matrix as a function of time; however, for the purpose of this paper, we will discuss the following physical quantities: $|\rho_{13}|$, $|\rho_{24}|$, and $|P_x|^2$. The excitation of the first two is a signature of nuclear CPT for the two Λ-systems. The absolute values of the coherences demonstrate the growth of the coherence and the establishment of nuclear CPT without distraction caused by their oscillatory nature. $|P_x|^2$ is the intensity of the polarization excited by the pulses, and it characterizes the response of the medium. It has the following relation to the elements of the density matrix

$$P_x \sim \frac{1}{\sqrt{2}}\left(\rho_{51} - \rho_{64}\right) + \frac{1}{\sqrt{6}}\left(\rho_{62} - \rho_{53}\right). \tag{5.5}$$

We will discuss the absolute square of this quantity only.

The broad bandwidth of the synchrotron radiation excites all (allowed) transi-

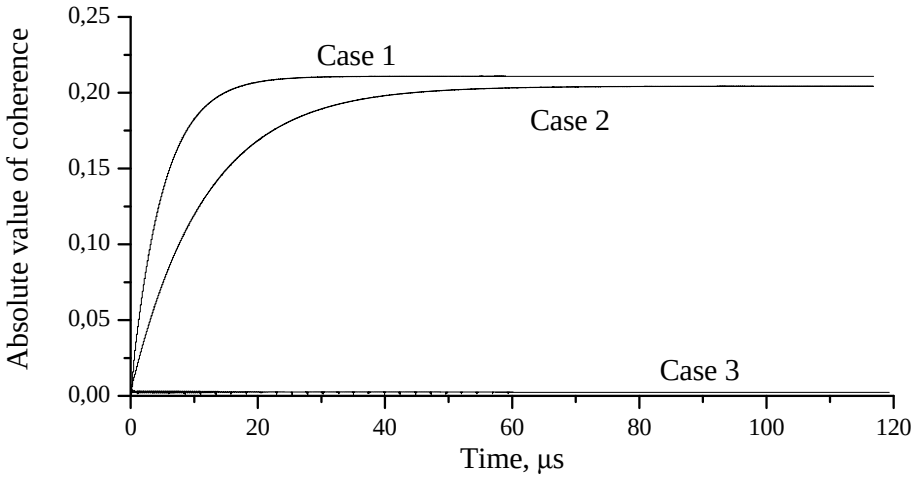

FIG. 32. The coherence between ground states for $\Omega_{max} = 1000\ rad/s$ without the assumption of random phases is presented. ρ_{13} and ρ_{24} are identical and are presented by the same line in each case. Difference between Case 1, Case 2 and Case 3 is discussed in the text.

tions. This excitation results in beating of P_x as time passes after the pulse arrival. In the time domain, the idea of CPT with a train of pulses is based on successive excitations of the system before the coherences have decayed completely; thus, $T_{decoherence} \gg T$. Such successive excitations have to have a proper timing to assure constructive interference of individual excitations; thus, $\Delta E_g = iT^{-1}$, where i is a positive integer. In the spectral domain, the idea of CPT with a train of pulses is based on the resonances of individual harmonics in the excitation spectrum of the periodic synchrotron radiation with the ground state separation, provided the selection rules allow such resonances.

Let us consider three cases. The first case, $2 \times \gamma_g B_z/2\pi = 1/0.153 = 2 \times 3.268$ MHz, is a primary resonance with $i = 1$ and corresponds to the separation of the ground levels 1(2) and 3(4) participating in the formation of the Λ-systems. The second case, $\gamma_g B_z/2\pi = 1/0.153 = 6.5359$ MHz, is a secondary resonance with

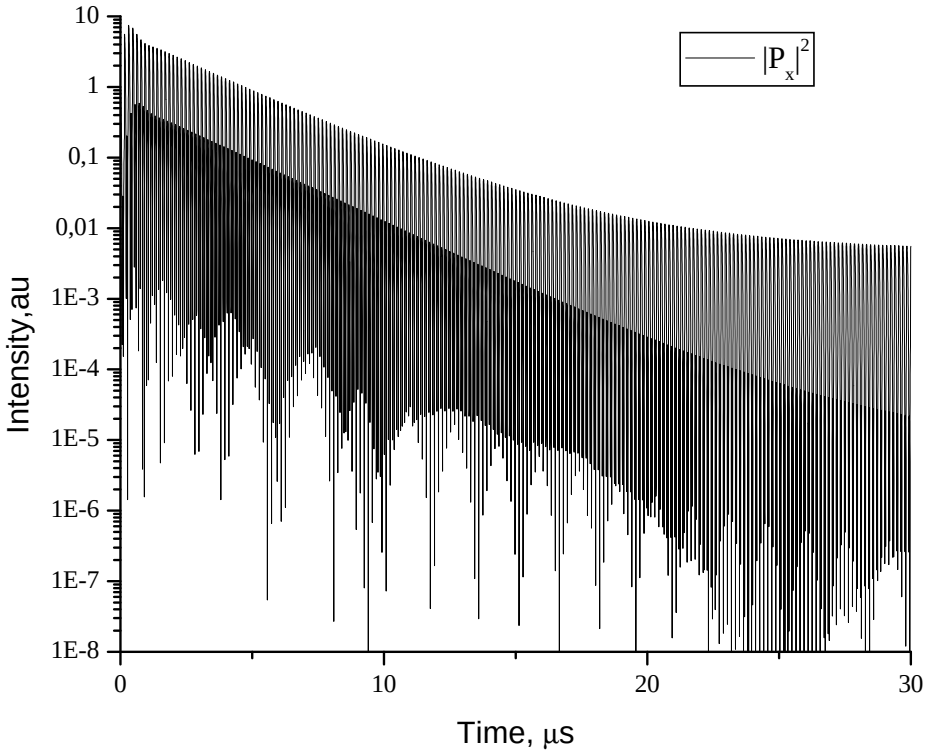

FIG. 33. The intensity of the nuclear polarization in the case of the primary resonance is presented and a pump with $\Omega_{max} = 1000\, rad/s$ is chosen. The corresponding coherences are discussed in Fig. 32. The first maximum is normalized to 1; however, a maximum of the order of 10 is reached after several initial pulses. The envelope of the polarization beating pattern demonstrates the suppression of the response of the system to the incoming radiation. A better view of the beating pattern can be found in Fig. 34.

$i = 2$. In this case, the resonance with the first harmonic is not relevant since it is forbidden due to selection rules; however, the second harmonic of the excitation spectrum matches the separation of the ground levels 1(2) and 3(4) participating in the formation of the Λ-systems, which also leads to nuclear CPT. The last case is an intermediate condition, $\gamma_g B_z/2\pi = 0.75/0.153 = 4.902$ MHz, when the resonant condition is not met.

In the first simulation, we assume that there is no phase change between pulses and a pump with $\Omega_{max} = 1000\ rad/s$. The coherences between the ground levels

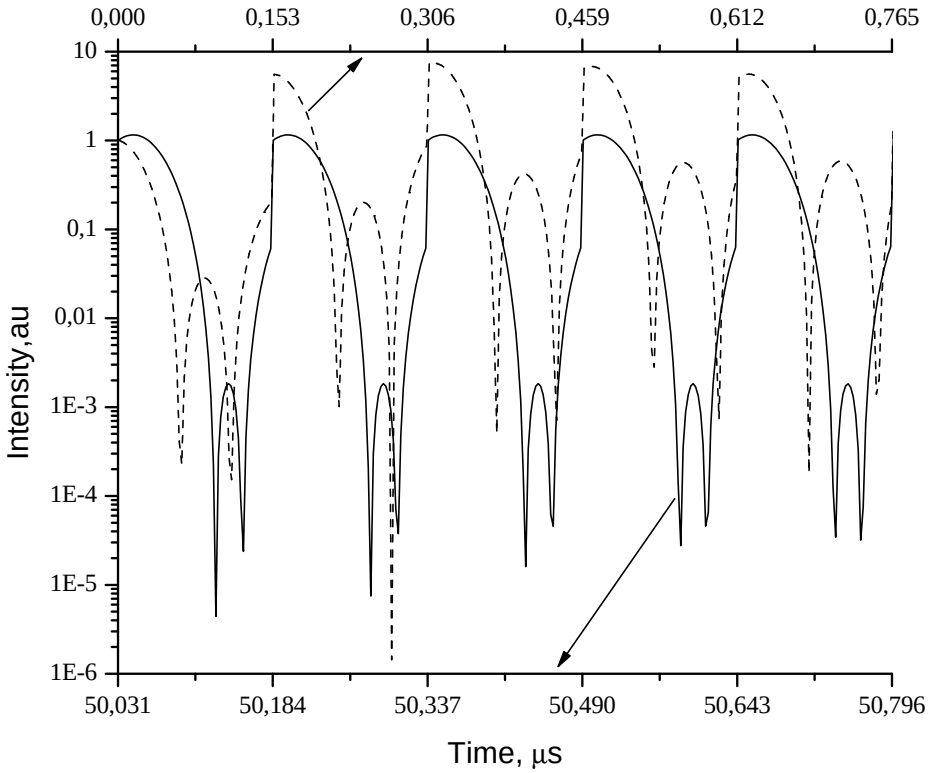

FIG. 34. The intensity of the nuclear polarization in the case of the primary resonance and a pump with $\Omega_{max} = 1000\, rad/s$ is presented. The dashed line presents the polarization during the first microsecond after arrival of the first pulse. The solid line presents the polarization normalized by $4.03 \cdot 10^{-3}$ after CPT is reached.

1(2) and 3(4) are identical and are shown in Fig. 32 by the solid lines. Efficient coherence build up is achieved only if the resonance condition for the first or the second harmonic of the excitation spectrum is met. As is expected, the coherence is created faster in the case of the primary resonance.

The creation of a coherent superposition of nuclear levels is a signature of nuclear CPT; however, it manifests itself in two different ways. The most common way is the suppression of the polarization and thus the nuclear elastic forward scattering. Figure 33 presents the nuclear polarization in the case of the primary resonance. One observes a beating pattern after each individual pulse and the envelope of $|P_x|^2$. The envelope shows that, although $|P_x(t=0)|^2 = 1$, $|P_x|^2$ reaches a maximum of the order of 10 soon after the arrival of the first pulse; however, it drops several orders of magnitude after thirty microseconds. Such a drop is a clear signature of CPT. The second manifestation of nuclear CPT is the modification of the beating pattern of the polarization decay. Figure 34 presents such a change. The dashed line is the polarization intensity during the first microsecond after arrival of the first pulse. It shows the amplification of the polarization after several pulses and the beating pattern. The solid line is the polarization intensity after nuclear CPT is established. This intensity is multiplied by a factor of $(4.03 \cdot 10^{-3})^{-1}$ to compensate for the suppression due to nuclear CPT and demonstrates the change in the time pattern of the polarization beating.

The main disadvantage of the first simulation is the assumption that the consecutive pulses have the same phase, which is not true in a real experiment. To address this concern, we introduce the assumption that consecutive pulses have random phases. The result of the simulations with random phases and $\Omega_{max} = 1000$ rad/s is presented in Fig. 35 in the case of the primary resonance and in the case when the resonant condition is not met. This result has to be compared directly with

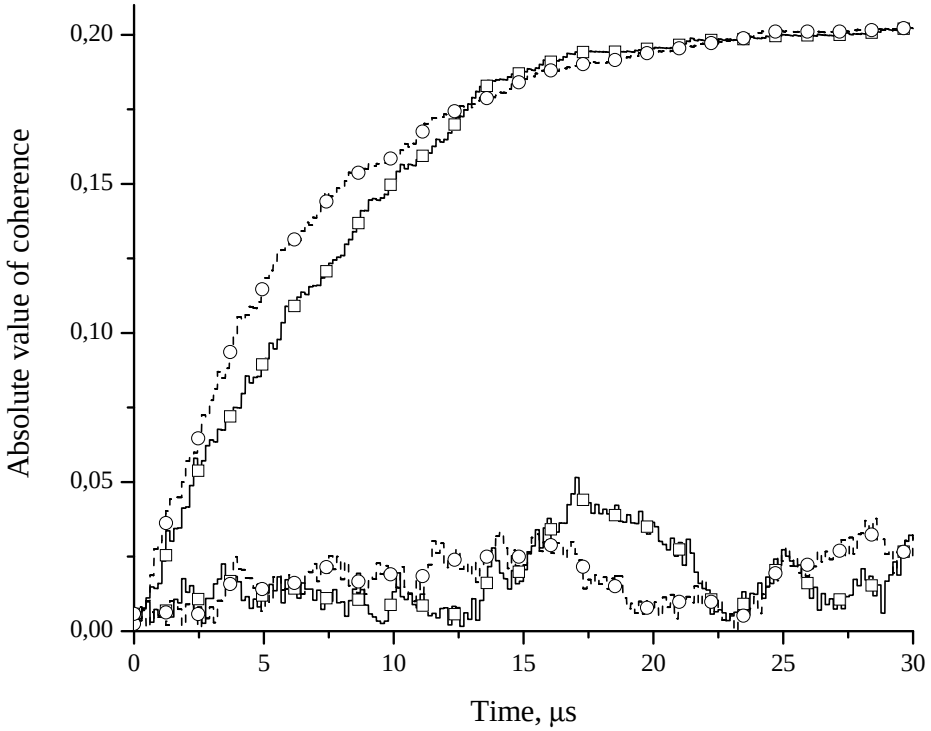

FIG. 35. Coherence between the ground states for a pump with $\Omega_{max} = 1000$ rad/s and a random phase shift. ρ_{13} and ρ_{24} are distinguishable as compared to the case of pulses with the same phases. ρ_{13} is presented by the solid line with squares. ρ_{24} is presented by the dashed line with circles.

the result in Fig. 32. The coherences ρ_{13} and ρ_{24} are distinguishable now. We do not show the case of the secondary resonance but it is almost identical with the case of the primary resonance. It can be seen that the coherence in the case of the primary resonance (1st case) reaches a maximum of 0.21, as it was under the assumption that consecutive pulses have the same phases, while the off-resonance case (3rd case) struggles to create a noticeable coherence but has a larger coherence than in the case when all pulses have the same phase. The explanation for this result is obvious if the spectral domain is considered. In this domain, the nuclear CPT is formed by a pair of harmonics in the excitation spectrum so that the frequency separation of the pair is equal to the separation of the ground states; thus, the relative phase of these two harmonics is important, not the absolute phase.

Finally, we want to draw attention to the intensities of the X-ray radiation necessary to create a substantial coherence. We assume no limitations for Ω_{max}; however, if one reduces this value by 10 with the corresponding reduction of the intensity by a factor of 100, much smaller coherences will be excited than those created by a stronger pump (see Fig. 36). It can be rectified if one assumes longer pulses than those that are typically available at the Advanced Photon Source at Argonne. Nevertheless, the synchrotron radiation with random pulses continues to excite the coherence almost as well as when all pulses have the same phases.

D. Conclusion

We demonstrated the possibility of nuclear CPT as well as suppression of nuclear elastic forward scattering with trains of ultrashort pulses of the synchrotron radiation. Several resonances can be used but the primary resonance can be considered as the most favorable one for synchronized pulses. We also addressed the issue of the phases

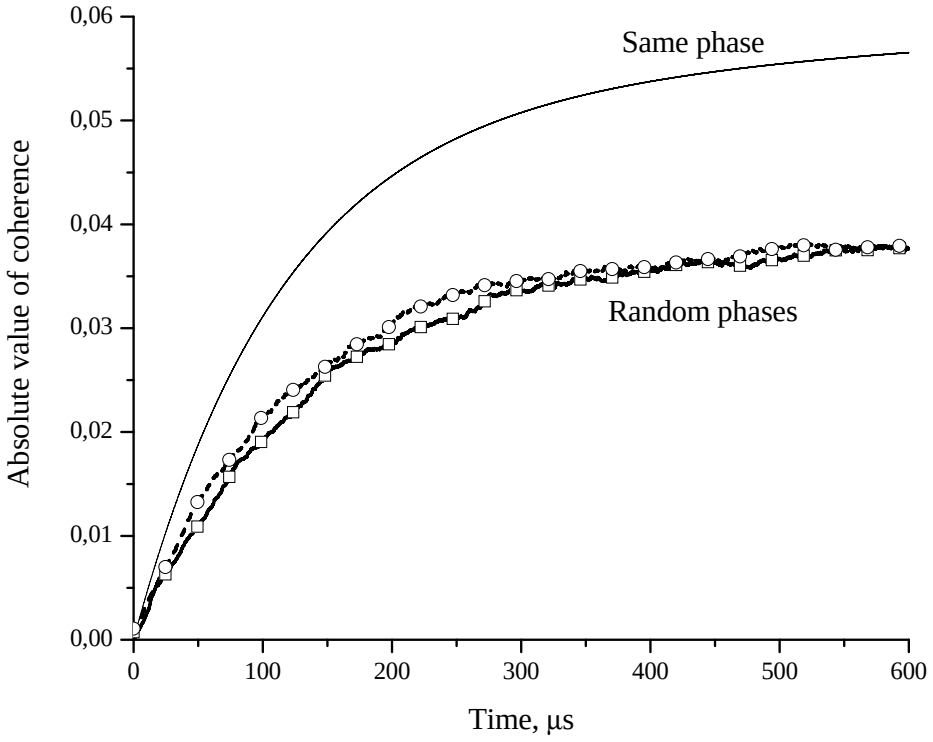

FIG. 36. Coherence between the ground states for a weaker pump with $\Omega_{max} = 100$ rad/s with and without a random phase shift in the case of the primary resonance.

of consecutive pulses, and showed that, as long as the periodicity was conserved, nuclear CPT was created; however, the primary and secondary resonances become indistinguishable.

CHAPTER VI

SUMMARY

The goal of this dissertation was to extend the quantum coherence phenomena, which are well-known in the optical frequency range, to a new field of X-ray optics and nuclear transitions. The major results are the following:

1. Analysis of the atomic response in resonant and off-resonant Λ-configurations is presented on the basis of the decaying dressed states. These states are introduced as the effective states which provide resonant contributions to the total atomic response. Such an approach has allowed for simple and straightforward classification of different regimes. The most interesting regime is for slow dephasing of two-photon coherence and sufficiently weak driving field. In this case, the decaying dressed states are dramatically different from the eigenstates of the "atom+field" Hamiltonian and especially useful for understanding the structure of the atomic response and its modifications with the variation of the parameters.

2. A simplified three-level model for the description of level-mixing induced transparency in $FeCO_3$ is suggested and analytically analyzed. It includes two crossing upper levels and a single lower level and assumes coupling between the crossing levels due to the axial symmetry breaking in the system. We have shown that the nuclear interference (similar to electromagnetically induced transparency at atomic transitions in optics) caused by this coupling may lead to suppression of the Mössbauer absorption at the level crossing point.

3. A new technique for suppression of inhomogeneous broadening of Mössbauer resonances is suggested. The suppression of the hyperfine contribution to the

width of Mössbauer resonances is due to the mutual compensation of the contributions of hyperfine interaction to the ground and excited states. This technique is based on the combined action of monochromatic RF and DC fields satisfying the modified "magic-angle" condition. Suggested modification was necessary to accommodate the specifics of the Mössbauer resonances. Nearly perfect suppression has been demonstrated numerically in a simple model involving a specific hyperfine interaction, namely the dipole-dipole interaction.

4. The possibility of coherent population trapping at nuclear transitions and its manifestation via suppression of nuclear elastic forward scattering with trains of ultrashort pulses of the synchrotron radiation was studied. Numerical simulations confirm such possibility. The main issued here has been the relative phases of consecutive pulses. The conclusion is that nuclear coherent population trapping is possible as long as the periodicity is maintained.

REFERENCES

[1] R. W. Wood and A. Ellet, Science **57**, 267 (1923).

[2] R. W. Wood and A. Ellett, Proc. Phys. Soc. (London) **103**, 396 (1923).

[3] R. W. Wood and A. Ellett, Phys. Rev. **24**, 243 (1924).

[4] W. Hanle, Zeitschrift für Physik **30**, 93 (1924).

[5] U. Fano, Phys. Rev. **124**, 1866 (1961).

[6] J. N. Dodd, W. N. Fox, G. W. Series, and M. J. Taylor, Proc. Phys. Soc. (London) **74**, 789 (1959).

[7] G. W. Series, Phys. Rev. A **136**, A684 (1964).

[8] A. Corney and G. W. Series, Proc. Phys. Soc. (London) **83**, 207 (1964).

[9] A. Corney and G. W. Series, Proc. Phys. Soc. (London) **83**, 213 (1964).

[10] S. Bashkin, W. S. Bickel, D. Fink, and R. K. Wangsnes, Phys. Rev. Lett. **15**, 284 (1965).

[11] R. L. Shoemake and R. G. Brewer, Phys. Rev. Lett. **28**, 1430 (1972).

[12] R. G. Brewer and E. L. Hahn, Phys. Rev. A **8**, 464 (1973).

[13] W. E. Bell and A. L. Bloom, Phys. Rev. Lett. **6**, 280 (1961).

[14] W. E. Bell and A. L. Bloom, Phys. Rev. Lett. **6**, 623 (1961).

[15] G. Alzetta, A. Gozzini, L. Moi, and G. Orriols, Nuovo Cimento Soc. Ital. Fis., B **36**, 5 (1976).

[16] H. R. Gray, R. M. Whitley, and C. R. Stroud, Opt. Lett. **3**, 218 (1978).

[17] Y. I. Heller and A. K. Popov, Opt. Commun. **18**, 7 (1976).

[18] Y. I. Heller, V. F. Lukinykh, A. K. Popov, and V. V. Slabko, Phys. Lett. A **82**, 4 (1981).

[19] P. L. Knight, M. A. Lauder, and B. J. Dalton, Phys. Rep. **190**, 1 (1990).

[20] E. Arimondo, in *Progress in Optics*, vol. 35, edited by E. Wolf (Elsevier, Amsterdam, 1996), pp. 257–354.

[21] D. Budker, W. Gawlik, D. F. Kimball, S. M. Rochester, V. V. Yashchuk, and A. Weis, Rev. Mod. Phys. **74**, 1153 (2002).

[22] O. A. Kocharovskaya and Y. I. Khanin, Zh. Eksp. Teor. Fiz. **90**, 1610 (1986).

[23] O. Kocharovskaya and P. Mandel, Phys. Rev. A **42**, 523 (1990).

[24] S. E. Harris, Phys. Today **50**, 36 (1997).

[25] J. P. Marangos, J. Mod. Opt. **45**, 471 (1998).

[26] O. Kocharovskaya, Phys. Rep. **219**, 175 (1992).

[27] A. B. Matsko, O. Kocharovskaya, Y. Rostovtsev, G. R. Welch, A. S. Zibrov, and M. O. Scully, Adv. At., Mol., Opt. Phys. **46**, 191 (2001).

[28] M. Fleischhauer, A. Imamoglu, and J. P. Marangos, Rev. Mod. Phys. **77**, 633 (2005).

[29] A. V. Turukhin, V. S. Sudarshanam, M. S. Shahriar, J. A. Musser, B. S. Ham, and P. R. Hemmer, Phys. Rev. Lett. **88**, 023602 (2002).

[30] R. Kolesov, Phys. Rev. A **72**, 051801 (2005).

[31] E. Kuznetsova, O. Kocharovskaya, P. Hemmer, and M. O. Scully, Phys. Rev. A **66**, 063802 (2002).

[32] R. Kolesov, M. O. Scully, and O. Kocharovskaya, Phys. Rev. A **74**, 053820 (2006).

[33] E. Kuznetsova, R. Kolesov, and O. Kocharovskaya, Phys. Rev. A **74**, 033804 (2006).

[34] O. Kocharovskaya, R. Kolesov, and Y. Rostovtsev, Phys. Rev. Lett. **82**, 3593 (1999).

[35] R. Kolesov, Y. Rostovtsev, and O. Kocharovskaya, Opt. Commun. **179**, 537 (2000).

[36] Y. Rostovtsev and O. Kocharovskaya, Hyperfine Interact. **135**, 233 (2001).

[37] Y. Rostovtsev, R. Kolesov, and O. Kocharovskaya, Hyperfine Interact. **143**, 121 (2002).

[38] F. Vagizov, R. Kolesov, S. Olariu, Y. Rostovtsev, and O. Kocharovskaya, Hyperfine Interact. **167**, 917 (2006).

[39] S. Olariu, R. Kolesov, F. Vagizov, and O. Kocharovskaya, J. Mod. Opt. **52**, 877 (2005).

[40] F. Vagizov, R. Kolesov, and O. Kocharovskaya, J. Mod. Opt. **51**, 2579 (2004).

[41] M. N. Hack and M. Hamermesh, Nuovo Cimento **19**, 546 (1961).

[42] A. V. Mitin, Sov. Phys. JETP **25**, 1062 (1967).

[43] A. V. Mitin, Opt. Spektrosk. **53**, 288 (1982).

[44] M. Salkola and S. Stenholm, Phys. Rev. A **41**, 3838 (1990).

[45] A. V. Mitin, Izv. Akad. Nauk SSSR, Ser. Fiz. **56**, 186 (1992).

[46] F. G. Vagizov, Hyperfine Interact. **61**, 1359 (1990).

[47] F. G. Vagizov, Hyperfine Interact. **61**, 1363 (1990).

[48] I. Tittonen, M. Lippmaa, E. Ikonen, J. Linden, and T. Katila, Phys. Rev. Lett. **69**, 2815 (1992).

[49] M. Lippmaa, I. Tittonen, K. Ullakko, and T. Katila, Hyperfine Interact. **71**, 1345 (1992).

[50] M. Lippmaa, I. Tittonen, J. Linden, and T. Katila, Nucl. Instrum. Methods Phys. Res., Sect. B **76**, 146 (1993).

[51] M. Lippmaa, I. Tittonen, J. Linden, and T. Katila, Hyperfine Interact. **92**, 1123 (1994).

[52] M. Lippmaa, I. Tittonen, J. Linden, and T. Katila, Phys. Rev. B **52**, 10268 (1995).

[53] L. Pfeiffer, J. Appl. Phys. **42**, 1725 (1971).

[54] M. Kopcewicz, H. G. Wagner, and U. Gonser, Solid State Commun. **48**, 531 (1983).

[55] A. Y. Dzyublik, V. Y. Spivak, R. A. Manapov, and F. G. Vagizov, JETP Lett. **67**, 61 (1998).

[56] P. Anisimov and O. Kocharovskaya, J. Mod. Opt. (2008), accepted.

[57] S. H. Autler and C. H. Townes, Phys. Rev. **100**, 703 (1955).

[58] A. Imamoglu and S. E. Harris, Opt. Lett. **14**, 1344 (1989).

[59] P. Anisimov, F. Vagizov, Y. Rostovtsev, R. Shakhmuratov, and O. Kocharovskaya, J. Mod. Opt. **54**, 2595 (2007).

[60] R. Coussement, Y. Rostovtsev, J. Odeurs, G. Neyens, H. Muramatsu, S. Gheysen, R. Callens, K. Vyvey, G. Kozyreff, P. Mandel, et al., Phys. Rev. Lett. **89**, 107601 (2002).

[61] J. Odeurs, R. Coussement, K. Vyvey, H. Muramatsu, S. Gheysen, R. Callens, G. Neyens, I. Serdons, R. N. Shakhmuratov, Y. Rostovtsev, et al., Hyperfine Interact. **143**, 97 (2002).

[62] S. Gheysen, R. Coussement, H. Muramatsu, R. N. Shakhmuratov, K. Vyvey, and J. Odeurs, J. Mod. Opt. **51**, 2589 (2004).

[63] R. N. Shakhmuratov, J. Odeurs, S. Gheysen, Y. Rostovtsev, O. Kocharovskaya, and P. Mandel, Appl. Phys. B **81**, 883 (2005).

[64] R. N. Shakhmuratov, J. Odeurs, S. Gheysen, Y. Rostovtsev, O. Kocharovskaya, and P. Mandel, Appl. Phys. B **83**, 635 (2006).

[65] S. Gheysen and J. Odeurs, Phys. Rev. B **74**, 155443 (2006).

[66] H. N. Ok, Phys. Rev. **185**, 472 (1969).

[67] M. O. Scully and M. S. Zubairy, *Quantum Optics* (Cambridge University Press, 1997).

[68] M. Blume and J. A. Tjon, Phys. Rev. **165**, 446 (1968).

[69] P. Anisimov, Y. Rostovtsev, and O. Kocharovskaya, Phys. Rev. B **76**, 094422 (2007).

[70] N. N. Greenwood and T. C. Gibb, *Mössbauer Spectroscopy* (Chapman and Hall, London, 1971).

[71] R. L. Cohen, *Applications of Mössbauer Spectroscopy* (Academic, New York, 1976).

[72] P. Gutlich, R. Link, and A. Trautwein, *Mössbauer Spectroscopy and Transition Metal Chemistry* (Springer-Verlag, Berlin, 1978).

[73] G. R. Hoy, *Encyclopedia of Physical Science and Technology*, vol. 10 (Academic, New York, 1992).

[74] G. J. Long and F. Grandjean, *Mössbauer Spectroscopy Applied to Magnetism and Materials Science* (Plenum, New York, 1993).

[75] J. Hesse and J. B. Muller, Solid State Commun. **22**, 637 (1977).

[76] D. G. Rancourt and J. Y. Ping, Hyperfine Interact. **69**, 497 (1991).

[77] L. A. Rivlin, Gamma-Ray Laser (1967), USSR patent disclosure.

[78] A. Andreev, Y. A. Il'inskii, and R. V. Khokhlov, Sov. Phys. JETP **40**, 819 (1975).

[79] G. C. Baldwin and J. C. Solem, Rev. Mod. Phys. **69**, 1085 (1997).

[80] U. Haeberlen, *High Resolution NMR in Solids: Selective Averaging* (Academic, New York, 1976).

[81] E. R. Andrew, A. Bradbury, and R. G. Eades, Nature (London) **182**, 1659 (1958).

[82] E. R. Andrew, A. Bradbury, and R. G. Eades, Nature (London) **183**, 1801 (1959).

[83] E. Hahn, Phys. Rev. **80**, 580 (1950).

[84] H. Carr and E. Purcell, Phys. Rev. **94**, 630 (1954).

[85] W. I. Goldburg and M. Lee, Phys. Rev. Lett. **11**, 255 (1963).

[86] Y. A. Il'inskii and R. V. Khokhlov, Sov. Phys. JETP **38**, 809 (1974).

[87] P. Anisimov, Y. Rostovtsev, and O. Kocharovskaya, J. Mod. Opt. **51**, 2615 (2004).

[88] P. Anisimov, Y. Rostovtsev, and O. Kocharovskaya, J. Mod. Opt. **52**, 2401 (2005).

[89] N. N. Greenwood and T. C. Gibb, *Mössbauer Spectroscopy* (Chapman and Hall, London, 1971), pp. 54–55.

[90] P. Meystre and M. Sargent, *Elements of Quantum Optics* (Springer, New York, 1999).

[91] E. U. Condon and G. H. Shortley, *The Theory of Atomic Spectra* (Cambridge University Press, Cambridge, England, 1935).

[92] I. Tittonen, M. Lippmaa, and J. Javanainen, Phys. Rev. A **53**, 1112 (1996).

[93] C. P. Slichter, *Principles of Magnetic Resonance*, 3rd ed. (Springer-Verlag, Berlin, 1990).

[94] P. Anisimov, Y. Rostovtsev, and J. Odeurs, J. Mod. Opt. **53**, 2459 (2006).

[95] J. P. Marangos, J. Mod. Opt. **45**, 471 (1998).

[96] J. Mompart and R. Corbalan, J. Opt. B **2**, R7 (2000).

[97] V. A. Sautenkov, Y. V. Rostovtsev, C. Y. Ye, G. R. Welch, O. Kocharovskaya, and M. O. Scully, Phys. Rev. A **71**, 063804 (2005).

[98] R. N. Zare, *Angular Momentum: Understanding Spatial Aspects in Chemistry and Physics* (Wiley, New York, 1988), p. 89.

APPENDIX A

CONCEPT OF EFFECTIVE MAGNETIC FIELD

Floquet analysis can be used to study behavior of the magnetic moment in the continuous wave RF and dc-magnetic fields $\mathbf{B}_{rf} = rB_0 \left(\cos\left(\omega_{rf}t\right)\mathbf{x}_0 - \sin\left(\omega_{rf}t\right)\mathbf{y}_0\right)$ and $\mathbf{B}_0 = B_0\mathbf{z}_0$ respectively. However, an equivalent description in terms of an effective magnetic field is more insightful.

The concept of the effective magnetic field may be introduced by carrying out a transformation to the co-rotating frame of reference $|old\rangle = R\left(-\omega_{rf}t\right)|new\rangle$, where $R\left(\theta\right) = e^{-i\theta\mathbf{I}\mathbf{z}_0}$ is a rotation operator with a direction of rotation along the z-axis. This transformation gives:

$$\frac{d}{dt}|new\rangle = -iH_{new}|new\rangle, \tag{A.1}$$

where $H_{new} = R^{-1}\left(-\omega_{rf}t\right)H_{old}R\left(-\omega_{rf}t\right) + \omega_{rf}I_z = -\gamma\mathbf{B}_{eff}$. Here we introduce the effective magnetic field $\mathbf{B}_{eff} = \left(rB_0, 0, B_0 - \frac{\omega_{rf}}{\gamma}\right)$. The effective magnetic field is time-independent and makes an angle with the z-axis $\theta_{eff} = \tan^{-1}\left(r\left(1 - \frac{\omega_{rf}}{\gamma B_0}\right)^{-1}\right)$. A Zeeman splitting corresponding to this field is $\Delta_{eff} = -\gamma\left|\mathbf{B}_{eff}\right| = \Delta\sqrt{\left(1 + \frac{\omega_{rf}}{\Delta}\right)^2 + r^2}$, where $\Delta = -\gamma\left|\mathbf{B}_0\right|$ is a Zeeman splitting in the lab frame. Thus, the eigenvalues are Zeeman splittings $E_n = m_{z,n}\Delta_{eff}$ in the effective magnetic field, and the eigenvectors are obtained by rotating the system around the y-axis by the angle θ_{eff}:

$$|n\rangle = \sum_{m=-I}^{I} d^I_{m,\,m_{z,n}}\left(\theta_{eff}\right)|m\rangle, \tag{A.2}$$

where a function $d^I_{m,m_{z,n}}\left(\theta_{eff}\right) = D^I_{m,m_{z,n}}\left(0, \theta_{eff}, 0\right)$ is an element of the rotation matrix [98].

An equivalence with Floquet analysis can be shown by a transformation to the lab frame. It gives:

$$|n,t\rangle = \sum_{m=-I}^{I} d^{I}_{m,\,m_{z,n}}\left(\theta_{eff}\right) e^{i\omega_{rf}tm}\,|m\rangle\,, \tag{A.3}$$

This is the Floquet state of the initially time-dependent Hamiltonian corresponding to a quasi-energy $E_n = \mod\ (m_{z,n}\Delta_{eff}, \omega_{rf})$.

If the system consists of two non-interacting subsystems, the Floquet states are obtained as a direct product of the Floquet states of individual subsystems $|n,t\rangle = |n_1,t\rangle \otimes |n_2,t\rangle$ with quasi-energy $E_n = E_{n_1} + E_{n_2}$.

APPENDIX B

THE PRESCRIPTION FOR THE FLOQUET ANALYSIS

According to the Floquet theorem in the case of periodic Hamiltonian $H_0(t)$, there is a set of time-dependent Floquet states $|n,t\rangle$ and corresponding quasi-energies ϵ_n which satisfy the following conditions: (i) each state is periodic in time $|n,t\rangle = |n,t+T\rangle$, where we have denoted the period by T; (ii) the quasi-energies and the Floquet states satisfy the Schrödinger equation

$$i\frac{\partial}{\partial t}\left(e^{-i\epsilon_n t}|n,t\rangle\right) = H_0(t)\left(e^{-i\epsilon_n t}|n,t\rangle\right). \tag{B.1}$$

In order to avoid inherent ambiguity in a definition of the Floquet states, we always assume that the corresponding quasi-energies are chosen in the interval $\epsilon_n \in \left[0, \omega_{rf} = \frac{2\pi}{T}\right)$. Furthermore, at any fixed time, the Floquet states may be chosen to form an orthonormal basis. This property allows us to write a time evolution operator in terms of the Floquet states as

$$U(t,0) = \sum_n e^{-i\epsilon_n t}|n,t\rangle\langle n,0|, \tag{B.2}$$

which obeys the equation $\dot{U}(t,0) = -iH_0(t)U(t,0)$ with an initial condition $U(0,0) = \hat{1}$. The first step is to diagonalize $U(T,0)$ because $U(T,0) = \sum_n e^{-i\epsilon_n T}|n,T\rangle\langle n,0|$ is diagonal in the basis of the Floquet states with eigenvalues $\lambda_n = e^{-i\epsilon_n T}$. It is true due to the periodicity condition $|n,T\rangle = |n,0\rangle$. The final step is to propagate the obtained states over the period $|n,t\rangle = e^{i\epsilon_n t}U(t,0)|n,0\rangle$, where we used $\epsilon_n = -\frac{1}{T}\arg(\lambda_n)$ shifted by ω_{rf} to fit the interval $\epsilon_n \in [0,\omega_{rf})$.

VITA

Petr Mikhailovich Anisimov

Department of Physics,
Texas A&M University,
c/o Dr. Olga Kocharovskaya,
College Station, TX 77843-4242.

Personal Information:

Born: 1977, Bor, Nizhegorodskaya obl, Russia.

Education:

Ph.D. in Physics, Texas A&M University, USA, December 2008.

M.S. in Physics, Summa Cum Laude, Nizhniy Novgorod State University, Russia, June 2001.

B.S. in Physics, Summa Cum Laude, Nizhniy Novgorod State University, Russia, June 1999.

The typist for this dissertation was Petr Mikhailovich Anisimov.